

Online Graph Topology Learning from Matrix-valued Time Series

Yiye Jiang^{1,2}, Jérémie Bigot¹ & Sofian Maabout²

¹Institut de Mathématiques de Bordeaux, Université de Bordeaux

²Laboratoire Bordelais de Recherche en Informatique, Université de Bordeaux

Abstract

This paper is concerned with the statistical analysis of matrix-valued time series. These are data collected over a network of sensors (typically a set of spatial locations), recording, over time, observations of multiple measurements. From such data, we propose to learn, in an online fashion, a graph that captures two aspects of dependency: one describing the sparse spatial relationship between sensors, and the other characterizing the measurements' relationship. To this purpose, we introduce a novel multivariate autoregressive model to infer the graph topology encoded in the coefficient matrix which captures the sparse Granger causality dependency structure present in such matrix-valued time series. We decompose the graph by imposing a Kronecker sum structure on the coefficient matrix. We develop two online approaches to learn the graph in a recursive way. The first one uses Wald test for the projected OLS estimation, where we derive the asymptotic distribution for the estimator. For the second one, we formalize a Lasso-type optimization problem. We rely on homotopy algorithms to derive updating rules for estimating the coefficient matrix. Furthermore, we provide an adaptive tuning procedure for the regularization parameter. Numerical experiments using both synthetic and real data, are performed to support the effectiveness of the proposed learning approaches.

1 Introduction

The identification of graph topology responds to increasing needs of data representation and visualization in many disciplines, such as meteorology, finance, neuroscience and social science. It is crucial to reveal the underlying relationships between data entries, even in the settings where the natural graphs are available. For example in Mei & Moura [13], the temperature graph that is inferred from the collection of multivariate time series recording temperature of cities around the continental United States over one-year period, differs from the distance graph, yet the former exhibiting a better performance in predicting weather trends. Many methods have been proposed to infer graphs for various data processes and application settings [4, 17]. The problem of graph

learning is to construct a graph \mathcal{G} from a collection of data such as random variables or time series, based on their observations $\mathbf{x}_t := (\cdots, x_{i,t}, \cdots)^\top$. The graph \mathcal{G} usually governs the data generating process $\mathcal{F}(\mathcal{G})$ of \mathbf{x}_t , where the edges represent the significant relationship among the coordinates of \mathbf{x}_t , considered as nodes in the graph. According to the data model $\mathcal{F}(\mathcal{G})$ and the definitions of edges, there are three main lines of work in graph learning domains.

The first line assumes that $\mathbf{x}_t \in \mathbb{R}^m$ is a vector-valued stationary process, where the edges are defined by the conditional dependence between its coordinates. Such models are known as Gaussian graphical models [6, 14], where \mathbf{x}_t is assumed to be independent and identically distributed from $\mathcal{N}(\mathbf{0}, \Theta^{-1})$, and the precision matrix Θ is assumed to be sparse so as to encode the effective graph topology. Bach & Jordan [1] and Songsiri & Vandenberghe [18] propose the graph learning approaches for stationary multivariate time series \mathbf{x}_t , and infer the conditional dependence graph from the inverse of its matrix-valued spectrum.

The second line is for multivariate autoregressive process \mathbf{x}_t with edges defined by Granger causality between its coordinate univariate time series $x_{i,t}$, see for example Bolstad et al. [2] and Mei & Moura [13]. The models impose identical sparsity through all coefficient matrices, and retrieve a graph from this sparse pattern. The learned graphs in this line are called causal graphs. They can be used to assist data processing tasks especially forecasting.

The third line focuses on employing the tools from the graph signal processing domain, like graph Laplacians, and impose data assumptions that can be characterized by these tools, such as smoothness [3, 10]. These approaches do not model the temporal structure of observations.

The success of the above-mentioned works encourages the generalization of graph learning methods for tensor-valued data $\mathbf{X}_t \in \mathbb{R}^{m_1 \times \cdots \times m_K}$. The main challenge for such generalization is the high-dimensionality of the resulting models in contrast with the limited sample size, due to the quadratic growth of the number of edges with respect to the graph size $\prod_{k=1}^K m_k$. One common technique is imposing a sparsity structure on the graph to reduce the number of parameters to be learned, and to obtain a more interpretable representation. In addition, it can be more realistic, since in many networks, each node interacts with only a small subset of other nodes.

Recent works have successfully extended the first line approach to the cases of matrix-valued [9] or tensor-valued data [8, 19]. To do so, a specific sparse structure is imposed on the graph by using a Kronecker product or Kronecker sum decomposition. Such models furthermore learn the sparse component graph along each mode k of the tensor. Additionally, to reduce the model complexity, the large graph can be interpreted immediately as the product graph of the component graphs.

In this paper, we introduce a novel structured multivariate autoregressive model $\mathcal{F}(\mathcal{G})$ for stationary and matrix-valued time series $\mathbf{X}_t \in \mathbb{R}^{N \times F}$, collecting the observations of N sensors for F measurements. The causal graph is inferred from a large coefficient matrix $\mathbf{A} \in \mathbb{R}^{NF \times NF}$. We adopt a similar technique to reduce the model complexity by decomposing \mathbf{A} into the Kronecker sum of two component causal graphs. In this setting, the main novel contribution of this work is to perform graph learning in an online fashion. To this end, we propose two online approaches to update the previously learned graphs with the streaming samples. One is based on the projected

OLS estimator and Wald test, the other one is based on a novel Lasso-type problem and the induced homotopy algorithms. For the regularization parameter in the Lasso approach, we also provide an automatic tuning procedure. On the other hand, to serve for the real applications where the observed time series are not stationary and cannot be detrended in a preliminary step, we propose an augmented data model to consider both the periodic trends and the graph as parameters. In this framework, we adapt the corresponding algorithms to update the trends and the graph simultaneously. To our best knowledge, this is the first work dedicated to online algorithms for graph learning for matrix-variate time series, which extends the second line of approaches mentioned above. Especially, we notice that the graphs learned by the second lines are usually directed. However this disables their use in those follow-up models which require undirected graphs as prior knowledge, like kernel methods, and graph Fourier transform related methods. Thus, to furthermore increase the applicability of the graph learning methods in this work, we focus on learning undirected graphs, with possible negative weights.

Outlines In the rest of this paper, we first present the aforementioned structured multivariate autoregressive model in Section 2, and we relate its graphical properties to Granger causality. We also provide the closed form of the projection operator onto the constrained coefficient space that is a key tool in the derivation of the two learning approaches considered in this paper. In Section 3, we develop these learning approaches in an online fashion. In Section 4, we propose the augmented data model, and we adapt the previous online approaches to this setting. Lastly, we present the results from numerical experiments using both synthetic and real data in Section 5. All proofs are gathered in a technical Appendix.

Notations We use $()$ to denote scalars and $[\]$ to denote vectors. Hence, $(\mathbf{v})_k$ denotes the k -th element of a vector \mathbf{v} , and $(\mathbf{M})_{i,j}$ denotes the (i, j) -th element of a matrix \mathbf{M} . For ordered indices $K = (\cdots, k_i, \cdots)$, $K' = (\cdots, k'_j, \cdots)$, $[\mathbf{v}]_K$ denotes the sub-vector $\tilde{\mathbf{v}}$, defined as $(\tilde{\mathbf{v}})_i = (\mathbf{v})_{k_i}$, and $[\mathbf{M}]_{K,K'}$ denotes the sub-matrix $\tilde{\mathbf{M}}$, defined as $(\tilde{\mathbf{M}})_{i,j} = (\mathbf{M})_{k_i,k'_j}$. When $K = K'$, we denote $[\mathbf{M}]_{K,K'}$ by $[\mathbf{M}]_K$. When $K = \{k_1\}$, we use k_1 directly in the above notations. Moreover, $[\mathbf{M}]_{:,i}$ denotes the i -th column vector of \mathbf{M} , and $\text{vec}(\mathbf{M})$ denotes the vectorization of matrix \mathbf{M} , that is, $\text{vec}(\mathbf{M}) = (\cdots, [\mathbf{M}]_{:,i}^\top, \cdots)^\top$. We denote by $\text{ivec}(\mathbf{v})$ the inverse operation of matrix vectorization, which recovers a matrix from a vector \mathbf{v} following the same order as $\text{vec}(\)$, and by $\text{svec}(\mathbf{M})$, the concatenation of the upper off-diagonal entries of \mathbf{M} into a vector, that is, $\text{svec}(\mathbf{M}) = ((\mathbf{M})_{1,2}, (\mathbf{M})_{1,3}, \cdots, (\mathbf{M})_{2,3}, \cdots)^\top$. We also denote by $\text{diag}(\mathbf{M})$ the vector whose i -th element is $(\mathbf{M})_{i,i}$, and by $\text{offd}(\mathbf{M})$ the matrix of the same size as \mathbf{M} , whose off-diagonal part is identical to that of \mathbf{M} , but its diagonal elements are equal to zero. The notation \mathbf{I}_d stand for the $d \times d$ identity matrix. Finally, $\mathbf{E}_k \in \mathbb{R}^{NF \times NF}$ denotes the matrix such that $(\mathbf{E}_k)_{k,k} = 1$ and all other elements equal to 0, while $\mathbf{e}_i \in \mathbb{R}^F$ (resp. $\mathbf{u}_j \in \mathbb{R}^N$) denotes the vector with i -th (resp. j -th) element equal to 1 and all others equal to 0.

2 Causality Product Graphs

We propose the following stable vector autoregressive model (VAR) for $\mathbf{X}_t \in \mathbb{R}^{N \times F}$ to retrieve the graph representation,

$$\mathbf{x}_t = \mathbf{A}\mathbf{x}_{t-1} + \mathbf{z}_t, \quad t \in \mathbb{Z}, \quad (2.1)$$

where $\mathbf{x}_t = \text{vec}(\mathbf{X}_t)$, $\mathbf{z}_t \in \mathbb{R}^{NF} \sim \text{IID}(\mathbf{0}, \boldsymbol{\Sigma})$ is a white noise vector with a non-singular covariance structure $\boldsymbol{\Sigma}$ and bounded fourth moments, and $\mathbf{A} \in \mathcal{K}_{\mathcal{G}}$ is the coefficient matrix with $\|\mathbf{A}\|_2 < 1$ that is constrained to belong to the set

$$\begin{aligned} \mathcal{K}_{\mathcal{G}} = & \{ \mathbf{M} \in \mathbb{R}^{NF \times NF} : \exists \mathbf{M}_F \in \mathbb{R}^{F \times F}, \mathbf{M}_N \in \mathbb{R}^{N \times N}, \text{ such that } \text{offd}(\mathbf{M}) = \mathbf{M}_F \oplus \mathbf{M}_N, \\ & \text{with } \mathbf{M}_F = \mathbf{M}_F^\top, \mathbf{M}_N = \mathbf{M}_N^\top, \text{diag}(\mathbf{M}_F) = \mathbf{0}, \text{diag}(\mathbf{M}_N) = \mathbf{0} \}. \end{aligned}$$

We define the causality graph \mathcal{G} as: each node $i = 1, \dots, NF$, represents a univariate time series $(\mathbf{x}_t)_i$, and there is an edge between node i and node j if and only if $(\mathbf{x}_t)_i$ and $(\mathbf{x}_t)_j$ constitutes a *feedback system*, that is, the two time series *Granger-cause* each other. The causality is defined in the sense that, $(\mathbf{x}_t)_j$ can be predicted more efficiently if the knowledge of $(\mathbf{x}_t)_i$ in the past and present is taken into account in the predictor in addition to all other information. For the stable VAR model, time series i causes j if and only if $(\mathbf{A})_{j,i} \neq 0$ [11, Corollary 2.2.1]. Thus, we can retrieve the graph topology from the sparse pattern in \mathbf{A} . In this work, we primarily focus on detecting the symmetric bivariate feedback systems (i, j) , which can be characterized by a single variable $(\mathbf{A})_{i,j} = (\mathbf{A})_{j,i}$. However, we stress that adapting the proposed approaches to other causality structures is straightforward.

Instead of inferring a fully-connected graph, constraining \mathbf{A} to belong to $\mathcal{K}_{\mathcal{G}}$ imposes a Cartesian product graph structure in $\text{offd}(\mathbf{A})$, and assumes that the dependency structure between all NF time series is essentially determined by the dependency among the N sensors which is invariant across measurements, and that the dependency between the F measurements is spatially invariant. These two aspects of dependencies can be represented by two respective causality graphs as well.

As described below in Equation (2.2), the matrix representation of Equation (2.1) clearly shows these two points. Indeed, applying $\text{ivec}(\cdot)$ on both sides of Equation (2.1), it follows that the relationship between \mathbf{X}_t and \mathbf{X}_{t-1} takes the form of a Sylvester-like equation:

$$\mathbf{X}_t = \mathbf{D} \circ \mathbf{X}_{t-1} + \mathbf{A}_N \mathbf{X}_{t-1} + \mathbf{X}_{t-1} \mathbf{A}_F^\top + \mathbf{Z}_t, \quad (2.2)$$

where \circ is Hadamard product, $\mathbf{D} \in \mathbb{R}^{N \times F} = \text{ivec}(\text{diag}(\mathbf{A}))$, \mathbf{A}_N and \mathbf{A}_F are the component matrices satisfying $\text{offd}(\mathbf{A}) = \mathbf{A}_F \oplus \mathbf{A}_N$, and $\mathbf{Z}_t = \text{ivec}(\mathbf{z}_t)$.

We consider the diagonal and off-diagonal part of \mathbf{A} separately, primarily to address the non-identifiability problem of Kronecker sum, since $\mathbf{A}_F \oplus \mathbf{A}_N = (\mathbf{A}_F + c\mathbf{I}_F) \oplus (\mathbf{A}_N - c\mathbf{I}_N)$ holds for any scalar c . Also, $\text{diag}(\mathbf{A})$ can be free from the structure constraint. This brings more flexibility to the model. In model (2.2), $\mathbf{A}_N \mathbf{X}_{t-1}$ contributes to the dependency structure from

the spatial point of view, where each column of \mathbf{X}_{t-1} can be viewed as a graph signal on the same sensor graph \mathcal{G}_N whose adjacency matrix is \mathbf{A}_N . Similarly, each row of \mathbf{X}_{t-1} can be seen as a graph signal on the measurement graph \mathcal{G}_F , whose adjacency matrix is \mathbf{A}_F . Thus, \mathcal{G} is the Cartesian product graph $\mathcal{G}_N \square \mathcal{G}_F$, with the added self-loops on all nodes.

2.1 Orthonormal Basis and Projection Operator of \mathcal{K}_G

The constraint set \mathcal{K}_G in model (2.1) is a linear subspace of $\mathbb{R}^{NF \times NF}$, onto which we can define a unique projection operator Proj_G using the Frobenius norm $\|\cdot\|_F$:

$$\text{Proj}_G(\mathbf{A}) = \arg \min_{\mathbf{M} \in \mathcal{K}_G} \|\mathbf{A} - \mathbf{M}\|_F^2. \quad (2.3)$$

We first construct an orthonormal basis of \mathcal{K}_G , and the projection is then found using inner products with elements in this basis as detailed in Proposition 2.2.

Lemma 2.1. *The matrices $\{\mathbf{U}_k\}_{k=1}^{d_G}$ defined below form an orthonormal basis of \mathcal{K}_G , with $d_G = NF + \frac{1}{2}N(N-1) + \frac{1}{2}F(F-1)$ and*

$$\begin{aligned} \mathbf{U}_k &= \mathbf{E}_k, \quad k = 1, \dots, d_D \\ \mathbf{U}_k &= c_F (\mathbf{e}_{l_k} \mathbf{e}_{h_k}^\top + \mathbf{e}_{h_k} \mathbf{e}_{l_k}^\top) \otimes \mathbf{I}_N, \quad k - d_D = 1, \dots, d_F \\ \mathbf{U}_k &= c_N \mathbf{I}_F \otimes (\mathbf{u}_{l_k} \mathbf{u}_{h_k}^\top + \mathbf{u}_{h_k} \mathbf{u}_{l_k}^\top), \quad k - d_{DF} = 1, \dots, d_N \end{aligned}$$

where $c_F = \frac{1}{\sqrt{2N}}$, $c_N = \frac{1}{\sqrt{2F}}$, $d_D = NF$, $d_F = \frac{1}{2}F(F-1)$, $d_{DF} = NF + \frac{1}{2}F(F-1)$, $d_N = \frac{1}{2}N(N-1)$, and the indices in the above equations are given by

$$\begin{aligned} \{(l_k, h_k)\}_{k=d_D+1}^{d_D+d_F} &= \{(1, 2), (1, 3), \dots, (1, F), (2, 3), (2, 4), \dots, (2, F), \dots, (F-1, F)\}, \\ \{(l_k, h_k)\}_{k=d_{DF}+1}^{d_{DF}+d_N} &= \{(1, 2), (1, 3), \dots, (1, N), (2, 3), (2, 4), \dots, (2, N), \dots, (N-1, N)\}. \end{aligned}$$

We remark that any $\mathbf{M} \in \mathcal{K}_G$ consists in copies of d_G entities from $\text{diag}(\mathbf{M})$ and upper off-diagonal parts in \mathbf{M}_F and \mathbf{M}_N at different locations. It is easy to see that each \mathbf{U}_k corresponds to one such entity, and indicates its copies' locations in a $NF \times NF$ matrix. Thus the index of \mathbf{U}_k , denoted by $K := \{1, \dots, d_G\}$, provides also an index for these entities. Additionally, we denote the index of entities from \mathbf{M}_F by $K_N := \{1 + d_{DF}, \dots, d_G\}$. Since the copy locations for any two entries do not overlap, $\langle \mathbf{U}_k, \mathbf{U}_{k'} \rangle^1 = \delta_{kk'}$, and

$$\mathbf{M} = \sum_{k \in K} \langle \mathbf{U}_k, \mathbf{M} \rangle \mathbf{U}_k,$$

which leads to the following result. Hereafter, we use *entity* of \mathbf{M} to exclusively refer to one of its d_G defining entries together with the entry's value, but not to refer to one copy in \mathbf{M} .

¹Inner products in this paper are all Frobenius ones.

Proposition 2.2. For a matrix $\mathbf{A} \in \mathbb{R}^{NF \times NF}$, its orthogonal projection onto $\mathcal{K}_{\mathcal{G}}$ is given by

$$\text{Proj}_{\mathcal{G}}(\mathbf{A}) = \mathbf{A}_D + \mathbf{A}_F \oplus \mathbf{A}_N \quad (2.4)$$

with $\mathbf{A}_D \in \mathbb{R}^{NF \times NF}$ defined as $(\mathbf{A}_D)_{i,j} = 0, i \neq j, (\mathbf{A}_D)_{i,i} = (\text{diag}(\mathbf{A}))_i$, and

$$\mathbf{A}_F = \sum_{1 \leq r < s \leq F} \langle c_F^2 (\mathbf{e}_r \mathbf{e}_s^\top + \mathbf{e}_s \mathbf{e}_r^\top) \otimes \mathbf{I}_N, \mathbf{A} \rangle (\mathbf{e}_r \mathbf{e}_s^\top + \mathbf{e}_s \mathbf{e}_r^\top) \quad (2.5)$$

$$\mathbf{A}_N = \sum_{1 \leq l < h \leq N} \langle c_N^2 \mathbf{I}_F \otimes (\mathbf{u}_l \mathbf{u}_h^\top + \mathbf{u}_h \mathbf{u}_l^\top), \mathbf{A} \rangle (\mathbf{u}_l \mathbf{u}_h^\top + \mathbf{u}_h \mathbf{u}_l^\top). \quad (2.6)$$

We denote Equation (2.5) and (2.6) as $\mathbf{A}_F = \text{Proj}_{\mathcal{G}_F}(\mathbf{A})$, $\mathbf{A}_N = \text{Proj}_{\mathcal{G}_N}(\mathbf{A})$, respectively. The linearity of the coefficient space will be exploited in the following section.

3 Online Graph Learning

In this section, we develop two learning frameworks to estimate \mathbf{A} recursively. The first method is valid in the low dimensional learning regime, where the number of samples along time is assumed to be sufficiently large with respect to the number of parameters. By contrast, the second method based on a Lasso-type problem requires fewer samples, and it is thus adapted to a high-dimensional learning regime. Additionally, we focus on imposing sparsity on \mathbf{A}_N , since in many applications, the measurement graph \mathbf{A}_F has a very small size. Yet, the extensions are also straightforward to the case where both graphs are assumed to be sparse.

3.1 Approach 1: Projected OLS Estimators and Wald Test

Assume that we start receiving a time series $\mathbf{x}_0, \mathbf{x}_1, \dots, \mathbf{x}_t$ from time $\tau = 1$, then VAR model (2.1) can be estimated by the ordinary least squares (OLS) estimation, leading to the following estimator of \mathbf{A} :

$$\check{\mathbf{A}}_t = \hat{\mathbf{\Gamma}}_t(1) \left[\hat{\mathbf{\Gamma}}_t(0) \right]^{-1} \quad (3.1)$$

where $\hat{\mathbf{\Gamma}}_t(0) = \frac{1}{t} \sum_{\tau=1}^t \mathbf{x}_{\tau-1} \mathbf{x}_{\tau-1}^\top$ and $\hat{\mathbf{\Gamma}}_t(1) = \frac{1}{t} \sum_{\tau=1}^t \mathbf{x}_\tau \mathbf{x}_{\tau-1}^\top$ are respectively consistent estimators of autocovariances $\mathbf{\Gamma}(0)$ and $\mathbf{\Gamma}(1)$, with $\mathbf{\Gamma}(h) = \mathbb{E}(\mathbf{x}_t [\mathbf{x}_{t-h}]^\top)$, $h \geq 0$. Moreover, $\check{\mathbf{A}}_t$ enjoys the asymptotic properties [11, Section 3.2.2]:

- (a) $\check{\mathbf{A}}_t \xrightarrow{p} \mathbf{A}$,
- (b) $\sqrt{t} \text{vec}(\check{\mathbf{A}}_t - \mathbf{A}) \xrightarrow{d} \mathcal{N}(0, \mathbf{\Sigma}_{ols})$, where $\mathbf{\Sigma}_{ols} = [\mathbf{\Gamma}(0)]^{-1} \otimes \mathbf{\Sigma}$.

Algorithm 1 Bisection Wald Test for Zero Weights

Input: $\mathbf{x}_{t+1}, \mathbf{x}_t, \widehat{\mathbf{\Gamma}}_t(0), \widehat{\mathbf{\Gamma}}_t(1), [\widehat{\mathbf{\Gamma}}_t(0)]^{-1}, t$

Update: $\widehat{\mathbf{\Gamma}}_{t+1}(1) = \frac{t}{t+1}\widehat{\mathbf{\Gamma}}_t(1) + \frac{1}{t+1}\mathbf{x}_{t+1}\mathbf{x}_t^\top$, $\widehat{\mathbf{\Gamma}}_{t+1}(0) = \frac{t}{t+1}\widehat{\mathbf{\Gamma}}_t(0) + \frac{1}{t+1}\mathbf{x}_t\mathbf{x}_t^\top$,

$[\widehat{\mathbf{\Gamma}}_{t+1}(0)]^{-1} = \frac{t+1}{t}[\widehat{\mathbf{\Gamma}}_t(0)]^{-1} - \frac{t+1}{t} \frac{[\widehat{\mathbf{\Gamma}}_t(0)]^{-1}\mathbf{x}_t\mathbf{x}_t^\top[\widehat{\mathbf{\Gamma}}_t(0)]^{-1}}{t+\mathbf{x}_t^\top[\widehat{\mathbf{\Gamma}}_t(0)]^{-1}\mathbf{x}_t}$,

$\widehat{\mathbf{\Sigma}}_{t+1} = \widehat{\mathbf{\Gamma}}_{t+1}(0) - \widehat{\mathbf{\Gamma}}_{t+1}(1)\widehat{\mathbf{\Gamma}}_{t+1}(0)^{-1}\widehat{\mathbf{\Gamma}}_{t+1}(1)^\top$,

$\check{\mathbf{A}}_{t+1} = \widehat{\mathbf{\Gamma}}_{t+1}(1)[\widehat{\mathbf{\Gamma}}_{t+1}(0)]^{-1}$.

Projection: $\widehat{\mathbf{A}}_{t+1} = \text{Proj}_{\mathcal{G}}(\check{\mathbf{A}}_{t+1})$, retrieve $\widehat{\mathbf{A}}_{\text{D},t+1}, \widehat{\mathbf{A}}_{\text{F},t+1}, \widehat{\mathbf{A}}_{\text{N},t+1}$ using Equation (2.4).

Sort the upper off-diagonal entries of $\widehat{\mathbf{A}}_{\text{N},t+1} : |(\widehat{\mathbf{A}}_{\text{N},t+1})_{i_1,j_1}| \leq \dots \leq |(\widehat{\mathbf{A}}_{\text{N},t+1})_{i_{d_{\text{N}}},j_{d_{\text{N}}}}|$.

Bisection Wald test procedure:

Initialize $p_l = 1$, $p_r = d_{\text{N}}$, $p_m = \text{Floor}(\frac{p_l+p_r}{2})$.

Construct the corresponding test statistic $\lambda_{W,t+1}$ or $\lambda_{F,t+1}$ using Equation (3.3).

Perform tests $H(1)$ and $H(d_{\text{N}})$ based on Corollary 3.1.1.

if $H(1)$, $H(d_{\text{N}})$ are not rejected: $\widehat{\mathbf{A}}_{\text{N},t+1} = 0$,

else

if $H(1)$, $H(d_{\text{N}})$ are both rejected: No changes are made to $\widehat{\mathbf{A}}_{\text{N},t+1}$,

else

while $p_l + 1 < p_r$:

$p_m \leftarrow \text{Floor}(\frac{p_l+p_r}{2})$, perform $H(p_m)$.

if $H(p_m)$ is not rejected: $p_l \leftarrow p_m$,

else: $p_r \leftarrow p_m$.

Let $(\widehat{\mathbf{A}}_{\text{N},t+1})_{i_1,j_1} = \dots = (\widehat{\mathbf{A}}_{\text{N},t+1})_{i_{p_l},j_{p_l}} = 0$.

$\widehat{\mathbf{A}}_{t+1} \leftarrow \widehat{\mathbf{A}}_{\text{D},t+1} + \widehat{\mathbf{A}}_{\text{F},t+1} \otimes \widehat{\mathbf{A}}_{\text{N},t+1}$.

$t \leftarrow t + 1$.

Output: $\widehat{\mathbf{A}}_{t+1}, \widehat{\mathbf{\Gamma}}_{t+1}(0), \widehat{\mathbf{\Gamma}}_{t+1}(1), \widehat{\mathbf{\Gamma}}_{t+1}(0)^{-1}, t$.

However, due to model misspecification and limited samples, $\check{\mathbf{A}}_t$ will not have the same structure as \mathbf{A} . Therefore, the projection of $\check{\mathbf{A}}_t$ onto $\mathcal{K}_{\mathcal{G}}$ needs to be performed, which leads to the projected OLS estimator:

$$\widehat{\mathbf{A}}_t := \text{Proj}_{\mathcal{G}}(\check{\mathbf{A}}_t),$$

with $\text{diag}(\mathbf{A})$, \mathbf{A}_{F} , and \mathbf{A}_{N} estimated by $\text{diag}(\check{\mathbf{A}}_t)$, $\text{Proj}_{\mathcal{G}_{\text{F}}}(\check{\mathbf{A}}_t)$, and $\text{Proj}_{\mathcal{G}_{\text{N}}}(\check{\mathbf{A}}_t)$, respectively, denoted by $\widehat{\mathbf{A}}_{\text{D},t}$, $\widehat{\mathbf{A}}_{\text{F},t}$, and $\widehat{\mathbf{A}}_{\text{N},t}$. To retrieve a sparse sensor graph, we propose to perform Wald test to identify the zero entries of \mathbf{A}_{N} . We first provide in Theorem 3.1 the asymptotic distribution of $\widehat{\mathbf{A}}_{\text{N},t}$.

Theorem 3.1. *The following central limit theorem (CLT) holds for $\widehat{\mathbf{A}}_{\text{N},t}$, as $t \rightarrow +\infty$,*

$$\sqrt{t} \text{svec}(\widehat{\mathbf{A}}_{\text{N},t} - \mathbf{A}_{\text{N}}) \xrightarrow{d} \mathcal{N}(0, \mathbf{\Sigma}_{\text{N}}), \quad (3.2)$$

where

$$\Sigma_N = \sum_{\substack{1 \leq l < h \leq N \\ 1 \leq l' < h' \leq N}} c_N^4 \tilde{\mathbf{u}}_{lh}^\top \Sigma_{ols} \tilde{\mathbf{u}}_{l'h'} \mathbf{E}_{lh'l'h'},$$

with $\mathbf{E}_{lh'l'h'} = \text{svec}(\mathbf{u}_l \mathbf{u}_h^\top) \text{svec}(\mathbf{u}_{l'} \mathbf{u}_{h'}^\top)^\top$, $\tilde{\mathbf{u}}_{lh} = \text{vec}(\mathbf{I}_F \otimes \mathbf{u}_l \mathbf{u}_h^\top + \mathbf{I}_F \otimes \mathbf{u}_h \mathbf{u}_l^\top)$, and $\tilde{\mathbf{u}}_{l'h'} = \text{vec}(\mathbf{I}_F \otimes \mathbf{u}_{l'} \mathbf{u}_{h'}^\top + \mathbf{I}_F \otimes \mathbf{u}_{h'} \mathbf{u}_{l'}^\top)$.

The proof is done through applying Cramér-Wold theorem on $\sqrt{t} \text{svec}(\widehat{\mathbf{A}}_{N,t} - \mathbf{A}_N)$, given the linearity of $\text{Proj}_{\mathcal{G}_N}(\mathbf{A})$, see Appendix A. The covariance between $(\widehat{\mathbf{A}}_{N,t} - \mathbf{A}_N)_{l,h}$ and $(\widehat{\mathbf{A}}_{N,t} - \mathbf{A}_N)_{l',h'}$ is assigned with the mean of covariances between the OLS estimators at their copies' locations, namely $c_N^4 \tilde{\mathbf{u}}_{lh}^\top \Sigma_{ols} \tilde{\mathbf{u}}_{l'h'}$, which follows the interpretation of Equation (2.4). In a similar way, it is possible to derive the asymptotic distribution of $\widehat{\mathbf{A}}_t$.

Based on this large sample result, we now derive the asymptotic distribution of a statistic to test of the nullity of P given entries $(\mathbf{A}_N)_{i_k, j_k}$, $k = 1, \dots, P$, with $i_k < j_k$, that is in term of hypothesis testing

$$H_0 : \alpha = 0 \text{ versus } H_1 : \alpha \neq 0$$

where $\alpha \in \mathbb{R}^P := (\dots, (\mathbf{A}_N)_{i_k, j_k}, \dots)^\top$. The test statistic is given by:

$$\lambda_{W,t} = t \hat{\alpha}_t^\top \left[\widehat{\Sigma}_{W,t} \right]^{-1} \hat{\alpha}_t, \quad (3.3)$$

where $\hat{\alpha}_t \in \mathbb{R}^P := (\dots, (\widehat{\mathbf{A}}_{N,t})_{i_k, j_k}, \dots)^\top$, $\widehat{\Sigma}_{W,t} \in \mathbb{R}^{P \times P}$ defined as: $(\widehat{\Sigma}_{W,t})_{k,k'} = c_N^4 \tilde{\mathbf{u}}_{i_k j_k}^\top \widehat{\Sigma}_{ols,t} \tilde{\mathbf{u}}_{i_{k'} j_{k'}}$, with the consistent estimators $\widehat{\Sigma}_{ols,t} = [\widehat{\Gamma}_t(0)]^{-1} \otimes \widehat{\Sigma}_t$, and $\widehat{\Sigma}_t = \widehat{\Gamma}_t(0) - \widehat{\Gamma}_t(1) [\widehat{\Gamma}_t(0)]^{-1} \widehat{\Gamma}_t(1)^\top$.

Corollary 3.1.1. *The asymptotic distribution of $\lambda_{W,t}$ is given by (as $t \rightarrow +\infty$)*

$$\lambda_{W,t} \xrightarrow{d} \chi^2(P), \quad \text{Under } H_0.$$

Remark 1. *We can also consider the test statistic $\lambda_{F,t} := \lambda_{W,t}/P$ as suggested in Lütkepohl [11, Section 3.6] in conjunction with the critical values from $F(P, t - NF - 1)$.*

Remark 2. *Since multiplication with $\tilde{\mathbf{u}}_{lh}$ amounts to extracting elements in the matrix from the corresponding locations, in practice, we take the elements directly from $[\widehat{\Gamma}_t(0)]^{-1}$ and $\widehat{\Sigma}_t$, to compose $\widehat{\Sigma}_{W,t}$ as:*

$$\left(\widehat{\Sigma}_{W,t} \right)_{k,k'} = \left(\widehat{\Sigma}_{W,t} \right)_{k',k} = \langle \Sigma_{ii}^{k,k'}, \Gamma_{jj}^{k,k'} \rangle + \langle \Sigma_{jj}^{k,k'}, \Gamma_{ii}^{k,k'} \rangle + \langle \Sigma_{ij}^{k,k'}, \Gamma_{ji}^{k,k'} \rangle + \langle \Sigma_{ji}^{k,k'}, \Gamma_{ij}^{k,k'} \rangle,$$

where $\Sigma_{ii}^{k,k'} = [\widehat{\Sigma}_t]_{I_k, I_{k'}}$, $\Gamma_{jj}^{k,k'} = [\widehat{\Gamma}_t(0)^{-1}]_{J_k, J_{k'}}$, $\Sigma_{jj}^{k,k'} = [\widehat{\Sigma}_t]_{J_k, J_{k'}}$, $\Gamma_{ii}^{k,k'} = [\widehat{\Gamma}_t(0)^{-1}]_{I_k, I_{k'}}$,
 $\Sigma_{ij}^{k,k'} = [\widehat{\Sigma}_t]_{I_k, J_{k'}}$, $\Gamma_{ji}^{k,k'} = [\widehat{\Gamma}_t(0)^{-1}]_{J_k, I_{k'}}$, and $\Sigma_{ji}^{k,k'} = [\widehat{\Sigma}_t]_{J_k, I_{k'}}$, $\Gamma_{ij}^{k,k'} = [\widehat{\Gamma}_t(0)^{-1}]_{I_k, J_{k'}}$,
with order indices $I_k := \{i_k, i_k + F, \dots, i_k + (N-1)F\}$, $I_{k'} := \{i_{k'}, i_{k'} + F, \dots, i_{k'} + (N-1)F\}$,
 $J_k := \{j_k, j_k + F, \dots, j_k + (N-1)F\}$, $J_{k'} := \{j_{k'}, j_{k'} + F, \dots, j_{k'} + (N-1)F\}$.

Instead of testing each entity in \mathbf{A}_N separately, we propose to test the p smallest entries of $\widehat{\mathbf{A}}_{N,t}$ jointly each time, as p grows from 1 to possibly largest value d_N . Specifically, for a given $\widehat{\mathbf{A}}_{N,t}$, we first sort its upper off-diagonal entries according to their absolute values, such that $|(\widehat{\mathbf{A}}_{N,t})_{i_1, j_1}| \leq \dots \leq |(\widehat{\mathbf{A}}_{N,t})_{i_{d_N}, j_{d_N}}|$. Then, we set up the sequence of tests: $H_0(1), H_0(2), \dots, H_0(d_N)$, where $H_0(p)$ denotes the null hypothesis: $\alpha(p) = 0$, with $\alpha(p) = \left((\widehat{\mathbf{A}}_{N,t})_{i_1, j_1}, \dots, (\widehat{\mathbf{A}}_{N,t})_{i_p, j_p} \right)^\top$. We can perform these tests sequentially until $H(p_0 + 1)$ is rejected for some p_0 . Lastly, we replace the entries $(\widehat{\mathbf{A}}_{N,t})_{i_1, j_1}, \dots, (\widehat{\mathbf{A}}_{N,t})_{i_{p_0}, j_{p_0}}$ with 0 in $\widehat{\mathbf{A}}_{N,t}$ as the final estimate of \mathbf{A}_N .

Note that in the procedure above, searching for p_0 resembles root-finding, since the output from each point p is binary. Thus, the search can be accelerated by using the bisection, with the maximal number of steps about $\log_2(d_N)$.

The previous procedure is performed at the t -th iteration, given the OLS estimator $\check{\mathbf{A}}_t$ and the consistent estimator $\check{\Sigma}_{ols,t}$. When the new sample pair $(\mathbf{x}_{t+1}, \mathbf{x}_t)$ comes, $\check{\mathbf{A}}_{t+1}$ and $\check{\Sigma}_{ols,t+1}$ can be calculated efficiently by applying *Sherman–Morrison formula* on $[\widehat{\Gamma}_t(0)]^{-1}$. We summarize the complete procedure in Algorithm 1.

3.2 Approach 2: Structured matrix-variate Lasso and Homotopy Algorithms

Another estimator of \mathbf{A} can be obtained by minimizing the following Lasso problem with matrix-valued parameters

$$\min_{\mathbf{A} \in \mathcal{K}_G} \frac{1}{2t} \sum_{\tau=1}^t \|\mathbf{x}_\tau - \mathbf{A}\mathbf{x}_{\tau-1}\|_{\ell_2}^2 + \lambda F \|\text{Proj}_{\mathcal{G}_N}(\mathbf{A})\|_{\ell_1}, \quad (3.4)$$

whose solution is denoted by $\mathbf{A}(t, \lambda)$. We also denote the above objective function by $L_{\lambda,t}$, and thus $A(t, \lambda) = \arg \min_{\mathbf{A} \in \mathcal{K}_G} L_{\lambda,t}(\mathbf{A})$.

When the new sample pair $(\mathbf{x}_{t+1}, \mathbf{x}_t)$ is available, our goal is to update the previous solution $\mathbf{A}(t, \lambda_t)$ to $\mathbf{A}(t+1, \lambda_{t+1})$, without solving the batch problem of $t+1$ samples. To this end, let us recall the formulation of the standard Lasso problem with vector-valued parameters:

$$\theta(t, \lambda) = \arg \min_{\theta \in \mathbb{R}^d} \frac{1}{2} \|\mathbf{y} - \mathbf{X}\theta\|_{\ell_2}^2 + t\lambda \|\theta\|_{\ell_1}, \quad (3.5)$$

where $\mathbf{y} \in \mathbb{R}^t$, and $\mathbf{X} \in \mathbb{R}^{t \times d}$ is the data matrix containing t samples. Many efficient algorithms have been proposed for updating $\theta(t, \lambda)$, when the regularization parameter or the data term

change. For example, methods in Efron et al. [5], Malioutov et al. [12] update the solution from $\theta(t, \lambda_1)$ to $\theta(t, \lambda_2)$, while Garrigues & Ghaoui [7] proposes an Homotopy algorithm which updates $\theta(t, \lambda_2)$ to $\theta(t + 1, \lambda_2)$. The adaptive λ selection rules, which update λ at the arrival of new samples are also studied in Garrigues & Ghaoui [7], Monti et al. [15]. Therefore, using the corresponding algorithms in the sequential updating steps:

$$\text{Step 1 : } \lambda_t \rightarrow \lambda_{t+1}, \quad \text{Step 2 : } \theta(t, \lambda) \rightarrow \theta(t, \lambda_{t+1}), \quad \text{Step 3 : } \theta(t, \lambda_{t+1}) \rightarrow \theta(t + 1, \lambda_{t+1}),$$

constitutes an online learning framework for the Lasso problem (3.5).

However, these existing methods are not applicable, when the updating steps above are related to Problem (3.4), due to the following significant differences between the two problems. For one thing, the coefficient matrix \mathbf{A} has a specific structure, for the other, the ℓ_1 regularization is imposed only on a subset of \mathbf{A} 's entries. Thus, in the rest of this section, we derive two homotopy algorithms, for the updating step $\mathbf{A}(t, \lambda_1) \rightarrow \mathbf{A}(t, \lambda_2)$ and $\mathbf{A}(t, \lambda_2) \rightarrow \mathbf{A}(t + 1, \lambda_2)$, respectively, together with the associated λ selection rules.

3.2.1 Optimality Conditions

The key point in deriving the optimality conditions arising from the variational problem (3.4) is to transfer the structure of \mathbf{A} onto the data vector $\mathbf{x}_{\tau-1}$, using an orthonormal basis of $\mathcal{K}_{\mathcal{G}}$. This enables us to compute the subdifferential $\frac{\partial L_{\lambda,t}}{\partial \mathbf{A}}$ in an easy way, and furthermore to retrieve a system of optimality conditions that is similar to the one derived from the standard Lasso problem (3.5). We elaborate on the derivation of this key point as follows.

We introduce the auxiliary variable \mathbf{A}^0 , such that $\mathbf{A} = \text{Proj}_{\mathcal{G}}(\mathbf{A}^0)$, and rewrite Problem (3.4) with respect to \mathbf{A}^0 :

$$\min_{\mathbf{A}^0 \in \mathbb{R}^{NF \times NF}} \frac{1}{2t} \sum_{\tau=1}^t \left\| \mathbf{x}_{\tau} - \sum_{k \in K} \langle \mathbf{U}_k, \mathbf{A}^0 \rangle \mathbf{U}_k \mathbf{x}_{\tau-1} \right\|_{\ell_2}^2 + \lambda \left\| \sum_{k \in K_N} \langle \mathbf{U}_k, \mathbf{A}^0 \rangle \mathbf{U}_k \right\|_{\ell_1}. \quad (3.6)$$

Problem (3.6) is weakly convex, since a minimizer of (3.4) can be projected from infinitely many minimizers of (3.6). We still use L_t to denote the objective function above. A minimizer \mathbf{A}^0 of (3.6) satisfies the optimality conditions:

$$0 \in \frac{\partial L_{\lambda,t}}{\partial \mathbf{A}^0} = \sum_{k,k' \in K} \langle \mathbf{U}_k, \mathbf{U}_{k'} \hat{\Gamma}_t(0) \rangle \langle \mathbf{U}_{k'}, \mathbf{A}^0 \rangle \mathbf{U}_k - \sum_{k \in K} \langle \mathbf{U}_k, \hat{\Gamma}_t(1) \rangle \mathbf{U}_k + 2\lambda F \sum_{k \in K_N} \partial |\langle \mathbf{U}_k, \mathbf{A}^0 \rangle| \mathbf{U}_k. \quad (3.7)$$

Equation (3.7) reveals the optimality condition for the optimisation problem (3.4), since $\langle \mathbf{U}_{k'}, \mathbf{A}^0 \rangle$ uniquely refers to an entity defining \mathbf{A} . On the other hand, because $\{\mathbf{U}_k\}_k$ is an orthonormal basis, by equating the values at copy locations of each \mathbf{U}_k in the matrices on the left hand side of the above equality to zero, an equation of all the entries can be retrieved. In this way, one obtains that $\mathbf{A}(t, \lambda)$ satisfies the optimality conditions stated in Proposition 3.2 below.

Notations of Proposition 3.2. Before stating this results, we need to introduce a few notation: we let $\mathbf{\Gamma}_0 \in \mathbb{R}^{d_{\mathcal{G}} \times d_{\mathcal{G}}}$ to be the matrix defined as $(\mathbf{\Gamma}_0)_{k,k'} = \langle c_k \mathbf{U}_k, c_{k'} \mathbf{U}_{k'} \widehat{\mathbf{\Gamma}}_t(0) \rangle$, and $\gamma_1 \in \mathbb{R}^{d_{\mathcal{G}}}$ to be defined as: $(\gamma_1)_k = \langle c_k \mathbf{U}_k, \widehat{\mathbf{\Gamma}}_t(1) \rangle$, with

$$c_k = \begin{cases} 1, & k = 1, \dots, NF \\ c_{\text{F}}, & k = 1 + d_{\text{D}}, \dots, d_{\text{DF}}, \\ c_{\text{N}}, & k = 1 + d_{\text{DF}}, \dots, d_{\mathcal{G}}. \end{cases}$$

We call $\{k \in K_{\text{N}} : (\mathbf{A}_{\text{N}})_{l_k, h_k} \neq 0, \mathbf{A}_{\text{N}} = \text{Proj}_{\mathcal{G}_{\text{N}}}(\mathbf{A}(t, \lambda))\}$ the *active set* of the matrix-variate Lasso problem (3.4), and denote it by K_{N}^1 . We also denote $K_{\text{N}}^0 := K_{\text{N}} \setminus K_{\text{N}}^1$ and $K^1 := K \setminus K_{\text{N}}^0$. Because the component orders of K^1, K_{N}^0 are used in the rest of this section. We use $i(k)$ to denote that, k is the $i(k)$ -th component of K^1 , for all $k \in K^1$, while $o(k)$ to denote that, k is the $o(k)$ -th component of K_{N}^0 , for all $k \in K_{\text{N}}^0$. Then we define

$$\mathbf{\Gamma}_0^1 = [\mathbf{\Gamma}_0]_{K^1}, \mathbf{\Gamma}_0^0 = [\mathbf{\Gamma}_0]_{K_{\text{N}}^0, K^1}, \gamma_1^1 = [\gamma_1]_{K^1}, \gamma_1^0 = [\gamma_1]_{K_{\text{N}}^0}.$$

$\mathbf{a}_1^s \in \mathbb{R}^{|K^1|}$ is defined as $(\mathbf{a}_1^s)_{i(k)} = \langle \frac{1}{c_k} \mathbf{U}_k, \mathbf{A}(t, \lambda) \rangle, k \in K^1$, which is the scaled Lasso solution for the active entities, and the entities $k = 1, \dots, d_{\text{DF}}$. We also let $\mathbf{w}_1 \in \mathbb{R}^{|K^1|} := (0, \mathbf{w}_{\text{N}}^1)^\top$, with $\mathbf{w}_{\text{N}}^1 \in \mathbb{R}^{|K_{\text{N}}^1|}$ defined as $(\mathbf{w}_{\text{N}}^1)_{i(k)-d_{\text{DF}}} = \text{sign} \langle \mathbf{U}_k, \mathbf{A}(t, \lambda) \rangle, k \in K_{\text{N}}^1$. Finally, we shall denote by $\mathbf{w}_0 \in \mathbb{R}^{|K_{\text{N}}^0|}$ a vector of subderivative whose elements belong to $[-1, 1]$.

Proposition 3.2. *The optimality conditions of the matrix-variate Lasso problem (3.4) is the following system of equations:*

$$\begin{cases} \mathbf{\Gamma}_0^1 \mathbf{a}_1^s - \gamma_1^1 + \sqrt{2F} \lambda \mathbf{w}_1 = 0 \\ \mathbf{\Gamma}_0^0 \mathbf{a}_1^s - \gamma_1^0 + \sqrt{2F} \lambda \mathbf{w}_0 = 0, \end{cases} \quad (3.8)$$

The optimality conditions (3.8) are similar to those of non-constrained multivariate Lasso [7, 12], where $\mathbf{\Gamma}_0, \gamma_1$ with the embedded structure correspond to $\mathbf{X}^\top \mathbf{X}, \mathbf{X}^\top \mathbf{y}$ in the optimality conditions of standard Lasso. However in our case, the non-zero and sign pattern are only with respect to the entries of \mathbf{A}_{N} , thus \mathbf{w}_1 , which is equivalent of the sign vector, has d_{DF} zeros.

3.2.2 Homotopy from $\mathbf{A}(t, \lambda_1)$ to $\mathbf{A}(t, \lambda_2)$

Suppose that $\mathbf{A}(t, \lambda)$ is the unique solution for a fixed λ of the optimisation problem (3.4), then, thanks to Proposition 3.2, we obtain that

$$\begin{cases} \mathbf{a}_1^s = [\mathbf{\Gamma}_0^1]^{-1} (\gamma_1^1 - \sqrt{2F} \lambda \mathbf{w}_1) \\ \sqrt{2F} \lambda \mathbf{w}_0 = \gamma_1^0 - \mathbf{\Gamma}_0^0 \mathbf{a}_1^s \end{cases} \quad (3.9)$$

Formula (3.9) is determined by the active set and the sign pattern of the optimal solution at λ . It shows that \mathbf{a}_1^s is a piecewise linear function of λ , while \mathbf{w}_0 is also a piecewise smooth function. Thus, with the assumptions that $(\mathbf{a}_1^s)_{i(k)} \neq 0, \forall k \in K_N^1$, and $|(\mathbf{w}_0)_{o(k)}| < 1, \forall k \in K_N^0$, due to continuity properties, there exists a range of values of λ , where for all λ' in this range, $[\mathbf{a}_1^s]_{K_N^1}$ remains nonzero with sign vector \mathbf{w}_N^1 unchanged, and \mathbf{w}_0 remains in $(-1, 1)$. Hence, the formula is the closed form of all the optimal solutions $\mathbf{A}(t, \lambda')$, for λ' in such range. This range is determined by the closest critical points to λ , which make either an entity of \mathbf{a}_1^s becomes zero, or an element of \mathbf{w}_0 reaches one in absolute value. By letting $[\mathbf{a}_1^s]_{K_N^1} = 0$ and $\mathbf{w}_0 = \pm 1$ in the respective formulas of (3.9), we can compute the critical values of λ as:

$$\begin{aligned}\lambda_k^0 &= \left([\mathbf{\Gamma}_0^1]^{-1} \gamma_1^1 \right)_{i(k)} / \left(\sqrt{2F} (\mathbf{\Gamma}_0^1)^{-1} \mathbf{w}_1 \right)_{i(k)}, \quad k \in K_N^1, \\ \lambda_k^+ &= \frac{\left(\gamma_1^0 - \mathbf{\Gamma}_0^0 [\mathbf{\Gamma}_0^1]^{-1} \gamma_1^1 \right)_{o(k)}}{\sqrt{2F} \left(1 - \mathbf{\Gamma}_0^0 (\mathbf{\Gamma}_0^1)^{-1} \mathbf{w}_1 \right)_{o(k)}}, \quad k \in K_N^0, \\ \lambda_k^- &= \frac{\left(\gamma_1^0 - \mathbf{\Gamma}_0^0 [\mathbf{\Gamma}_0^1]^{-1} \gamma_1^1 \right)_{o(k)}}{\sqrt{2F} \left(-1 - \mathbf{\Gamma}_0^0 (\mathbf{\Gamma}_0^1)^{-1} \mathbf{w}_1 \right)_{o(k)}}, \quad k \in K_N^0.\end{aligned}\tag{3.10}$$

Thus, the range of values for λ' is given by (λ_l, λ_r) , where

$$\begin{aligned}\lambda_l &:= \max \left\{ \max\{\lambda_k^0, k \in K_N^1 : \lambda_k^0 < \lambda\}, \max\{\lambda_k^+, k \in K_N^0 : \lambda_k^+ < \lambda\}, \max\{\lambda_k^-, k \in K_N^0 : \lambda_k^- < \lambda\} \right\}, \\ \lambda_r &:= \min \left\{ \min\{\lambda_k^0, k \in K_N^1 : \lambda_k^0 > \lambda\}, \min\{\lambda_k^+, k \in K_N^0 : \lambda_k^+ > \lambda\}, \min\{\lambda_k^-, k \in K_N^0 : \lambda_k^- > \lambda\} \right\}.\end{aligned}\tag{3.11}$$

If $\lambda_l = \emptyset$ then $\lambda_l := 0$, while if $\lambda_r = \emptyset$ then $\lambda_r := +\infty$. After λ' leaves the region by changing the active set and sign pattern, we reformulate the optimality conditions based on this change, and calculate the boundary of the new region as before. We proceed in this way until we reach the region covering the λ value at which we would like to calculate the Lasso solution, and use Formula (3.9) in this final region to compute the \mathbf{a}_1^s with the desired λ value. Lastly, we retrieve the matrix-form optimal solution based on \mathbf{a}_1^s and the associated K^1 . This completes the first homotopy algorithm. We summarize the main steps of the procedure in Algorithm 2.

3.2.3 Homotopy from $\mathbf{A}(t, \lambda)$ to $\mathbf{A}(t + 1, \lambda)$

In Garrigues & Ghaoui [7], a continuous variable μ is introduced in the standard Lasso formulation (3.5) leading to the optimization Problem (3.12) below

$$\min_{\theta \in \mathbb{R}^d} \frac{1}{2} \|\mathbf{y} - \mathbf{X}\theta\|_{\ell_2}^2 + \frac{1}{2} (\mu y_{t+1} - \mu \mathbf{x}_{t+1}^\top \theta)^2 + t\lambda \|\theta\|_{\ell_1},\tag{3.12}$$

in order to let evolve the problem of learning from t samples to that of learning from $t + 1$ samples, as μ goes from 0 to 1. In such a way, an homotopy algorithm can be derived which computes the path from $\theta(t, \lambda)$ to $\theta(t + 1, \lambda)$.

Algorithm 2 Homotopy Algorithm for Regularization Path

Input: $N, F, \mathbf{\Gamma}_0, \gamma_1, K_N^1, \mathbf{w}_N^1, \lambda_1, \lambda_2, [\mathbf{\Gamma}_0^1]^{-1}$, where $K_N^1, \mathbf{w}_N^1, [\mathbf{\Gamma}_0^1]^{-1}$ are associated with $\mathbf{A}(t, \lambda_1)$.

Initialization: $\lambda \leftarrow \lambda_1, K_N^0 \leftarrow K_N \setminus K_N^1, K^1 \leftarrow K \setminus K_N^0$.

Computing the regularization path (the steps in parentheses are the modifications for the case $\lambda_1 > \lambda_2$):

while $\lambda < \lambda_2$ (or $\lambda > \lambda_2$):

 Generate $\mathbf{\Gamma}_0^0, \gamma_1^1, \gamma_1^0, \mathbf{w}_1$, based on Proposition 3.2.

 Compute λ_r (or λ_l), based on Equation (3.10) and (3.11).

if $\lambda_r < \lambda_2$ (or $\lambda_l > \lambda_2$):

$\lambda = \lambda_r$ (or $\lambda = \lambda_l$),

 Update the active set and the sign vector:

if $(\mathbf{a}_1^s)_{i(k)}$ becomes zero for some $k \in K_N^1$, namely, λ comes from $\{\lambda_k^0\}_k$:

$K_N^1 \leftarrow K_N^1 \setminus \{k\}, K^1 \leftarrow K^1 \setminus \{k\}, K_N^0 \leftarrow K_N^0 \cup \{k\}$. Remove $(\mathbf{w}_N^1)_{i(k)-d_{DF}}$ from \mathbf{w}_N^1 .

 Remove the $i(k)$ -th row together with the $i(k)$ -th column from $\mathbf{\Gamma}_0^1$,

 and use block matrix inversion formula to update $[\mathbf{\Gamma}_0^1]^{-1}$.

if $(\mathbf{w}_0)_k$ reaches 1 for some $k \in K_N^0$, namely, λ comes from $\{\lambda_k^+\}_k$:

$K_N^0 \leftarrow K_N^0 \setminus \{k\}, K_N^1 \leftarrow K_N^1 \cup \{k\}, K^1 \leftarrow K^1 \cup \{k\}$. Append 1 to the end of sign

vector \mathbf{w}_N^1 .

 Append row $[\mathbf{\Gamma}_0]_{k, K^1}$, column $[\mathbf{\Gamma}_0]_{K^1, k}$ after the last row and last column $\mathbf{\Gamma}_0^1$,

respectively,

 and use block matrix inversion formula to update $[\mathbf{\Gamma}_0^1]^{-1}$.

if $(\mathbf{w}_0)_k$ reaches -1 for some $k \in K_N^0$, namely, λ comes from $\{\lambda_k^-\}_k$:

$K_N^0 \leftarrow K_N^0 \setminus \{k\}, K_N^1 \leftarrow K_N^1 \cup \{k\}, K^1 \leftarrow K^1 \cup \{k\}$. Append -1 to the end of sign

vector \mathbf{w}_N^1 .

 Append row $[\mathbf{\Gamma}_0]_{k, K^1}$, column $[\mathbf{\Gamma}_0]_{K^1, k}$ after the last row and last column $\mathbf{\Gamma}_0^1$,

respectively,

 and use block matrix inversion formula to update $[\mathbf{\Gamma}_0^1]^{-1}$.

else: $\lambda = \lambda_2$.

 Compute \mathbf{a}_1^s using Equation (3.9) and the last updated $[\mathbf{\Gamma}_0^1]^{-1}, \gamma_1^1, \mathbf{w}_1$. Retrieve $\mathbf{A}(t, \lambda_2)$ from this \mathbf{a}_1^s .

Output: $\mathbf{A}(t, \lambda_2), K_N^1, \mathbf{w}_N^1, [\mathbf{\Gamma}_0^1]^{-1}$.

This homotopy algorithm is derived based on the fact that, the term of new sample will only arise one rank change in the covariance matrix as $\mathbf{X}^\top \mathbf{X} + \mu^2 \mathbf{x}_{t+1}^\top \mathbf{x}_{t+1}$. Thus, the corresponding

matrix inverse in the closed form of optimal solution can be still expressed as an explicit function of μ using the Sherman-Morrison formula, which furthermore allows the calculation of transition points. However, for the matrix-variate Lasso (3.4), a new sample will cause NF rank change² in $\mathbf{\Gamma}_0$, since $\mathbf{\Gamma}_0 = \frac{1}{t} \sum_{\tau=1}^t \tilde{\mathbf{X}}_{\tau-1} \tilde{\mathbf{X}}_{\tau-1}^\top$, with $\tilde{\mathbf{X}}_{\tau-1} \in \mathbb{R}^{d_G \times NF}$ defined as $(\tilde{\mathbf{X}}_{\tau-1})_{k,i} = c_k [\mathbf{U}_k]_{i,:} \mathbf{x}_{\tau-1}$. Thus it is impossible to express $[\mathbf{\Gamma}_0^1]^{-1}$ as an explicit and simple function of a single μ . On the other hand, observe that

$$\|\mathbf{x}_{t+1} - \mathbf{A}\mathbf{x}_t\|_{\ell_2}^2 = \left\| \mathbf{x}_{t+1} - \sum_{k \in K} \langle \mathbf{U}_k, \mathbf{A}^0 \rangle \mathbf{U}_k \mathbf{x}_t \right\|_{\ell_2}^2 = \sum_{i=1}^{NF} (\mathbf{x}_{t+1,i} - \sum_{k \in K} [\mathbf{U}_k]_{i,:} \mathbf{x}_t \text{vec}(\mathbf{U}_k)^\top \text{vec}(\mathbf{A}^0))^2,$$

where we denote $\sum_{k \in K} [\mathbf{U}_k]_{i,:} \mathbf{x}_t \text{vec}(\mathbf{U}_k)^\top$ by $[\mathbf{X}'_t]_{i,:}$, $\mathbf{x}_{t+1,i} := (\mathbf{x}_{t+1})_i$ and $\mathbf{A} = \text{Proj}_{\mathcal{G}}(\mathbf{A}^0)$. Therefore, we propose to introduce NF continuous variables μ_1, \dots, μ_{NF} in the matrix-variate Lasso (3.4), and to consider the following problem:

$$\min_{\mathbf{A} \in \mathcal{K}_{\mathcal{G}}} \frac{1}{2(t+1)} \sum_{\tau=1}^t \|\mathbf{x}_{\tau} - \mathbf{A}\mathbf{x}_{\tau-1}\|_{\ell_2}^2 + \lambda F \|\text{Proj}_{\mathcal{G}_N}(\mathbf{A})\|_{\ell_1} + \frac{1}{2(t+1)} \sum_{i=1}^{NF} \mu_i (\mathbf{x}_{t+1,i} - [\mathbf{X}'_t]_{i,:} \text{vec}(\mathbf{A}^0))^2. \quad (3.13)$$

We denote the objective function above as $L_{\lambda,t}(\mu_1, \dots, \mu_{NF})$, with its solution denoted by $\mathbf{A}_{\lambda,t}(\mu_1, \dots, \mu_{NF})$. Given solution $\mathbf{A}(t, \lambda)$, we first apply Algorithm 2 on it with $\lambda_1 = \lambda$ and $\lambda_2 = \frac{t+1}{t}\lambda$ to change the constant before the old data term from $\frac{1}{t}$ to $\frac{1}{t+1}$. Then, we have $\mathbf{A}(t, \frac{t+1}{t}\lambda) = \mathbf{A}_{\lambda,t}(0, \dots, 0)$ and $\mathbf{A}(t+1, \lambda) = \mathbf{A}_{\lambda,t}(1, \dots, 1)$. We let evolving the optimisation problem (3.4) from time t to $t+1$ by sequentially varying all μ_i from 0 to 1, along the paths $L_{\lambda,t}(0, 0, \dots, 0) \rightarrow L_{\lambda,t}(1, 0, \dots, 0) \rightarrow L_{\lambda,t}(1, 1, \dots, 1) = L_{\lambda,t+1}$. The calculation of the optimal conditions shows that, each path only relates to the one rank change: $\frac{\mu_i}{t} [\tilde{\mathbf{X}}_t]_{:,i} [\tilde{\mathbf{X}}_t]_{:,i}^\top$, for the latest updated $\mathbf{\Gamma}_0$. This change corresponds to the new observation at node i in \mathcal{G} . Thus throughout these paths, the transition points of μ_i can be computed explicitly. We first provide the optimality conditions of Problem $L_{\lambda,t}(\dots, 1, \mu_i, 0, \dots)$ in Proposition 3.3 below, then summarize the algorithm which computes the path from $\mathbf{A}(t, \frac{t+1}{t}\lambda)$ to $\mathbf{A}(t+1, \lambda)$ in Algorithm 3. We recall the notations of Proposition 3.2: $\mathbf{a}_1^s, K_N^1, K_N^0, K^1, \mathbf{w}_1, \mathbf{w}_0$, which represent the sparsity and sign pattern of Lasso solution $\mathbf{A}(t, \lambda)$. In Proposition 3.3, we use the same notations to formalize the system optimality conditions, while they are related to the solution $\mathbf{A}_{\lambda,t}(\dots, 1, \mu_i, 0, \dots)$ here.

Proposition 3.3. *The optimality conditions of the optimisation problem with objective function $L_{\lambda,t}(\dots, 1, \mu_i, 0, \dots)$ (where only μ_i is allowed to vary) is the following system of equations:*

$$\begin{cases} \mathbf{\Gamma}_0^1(\mu_i) \mathbf{a}_1^s - \gamma_1^1(\mu_i) + (1 + \frac{1}{t}) \sqrt{2F} \lambda \mathbf{w}_1 = 0 \\ \mathbf{\Gamma}_0^0(\mu_i) \mathbf{a}_1^s - \gamma_1^0(\mu_i) + (1 + \frac{1}{t}) \sqrt{2F} \lambda \mathbf{w}_0 = 0, \end{cases} \quad (3.14)$$

²On the other hand, this implies that $\mathbf{\Gamma}_0$ will quickly become non-singular from the initial time, as new samples \mathbf{x}_{τ} come in.

where

$$\mathbf{\Gamma}_0(\mu_i) = \mathbf{\Gamma}_0 + \frac{1}{t} \sum_{n=1}^{i-1} [\tilde{\mathbf{X}}_t]_{:,n} [\tilde{\mathbf{X}}_t]_{:,n}^\top + \frac{\mu_i}{t} [\tilde{\mathbf{X}}_t]_{:,i} [\tilde{\mathbf{X}}_t]_{:,i}^\top, \quad (3.15)$$

and

$$\gamma_1(\mu_i) = \gamma_1 + \frac{1}{t} \sum_{n=1}^{i-1} \mathbf{x}_{t+1,n} [\tilde{\mathbf{X}}_t]_{:,n} + \frac{\mu_i}{t} \mathbf{x}_{t+1,i} [\tilde{\mathbf{X}}_t]_{:,i}, \quad (3.16)$$

with $\mathbf{\Gamma}_0, \gamma_1$ defined as Proposition 3.2, and $\mathbf{\Gamma}_0^1(\mu_i) = [\mathbf{\Gamma}_0(\mu_i)]_{K^1}$, $\mathbf{\Gamma}_0^0(\mu_i) = [\mathbf{\Gamma}_0(\mu_i)]_{K_{\mathbb{N}}^0, K^1}$, $\gamma_1^1(\mu_i) = [\gamma_1(\mu_i)]_{K^1}$, $\gamma_1^0(\mu_i) = [\gamma_1(\mu_i)]_{K_{\mathbb{N}}^0}$.

We apply the Sherman-Morrison formula on $[\mathbf{\Gamma}_0^1(\mu_i)]^{-1}$ to retrieve the smooth function of μ_i , and express \mathbf{a}_1^s and \mathbf{w}_0 as smooth functions of μ_i . To leverage these continuity properties, we still assume $(\mathbf{a}_1^s)_{i(k)} \neq 0$, $\forall k \in K_{\mathbb{N}}^1$, and $|(\mathbf{w}_0)_{o(k)}| < 1$, $\forall k \in K_{\mathbb{N}}^0$. For the algorithm of path $\mathbf{A}_{\lambda,t}(0, \dots, 0)$ to $\mathbf{A}_{\lambda,t}(1, \dots, 1)$, it is sufficient to impose such assumption only on $\mathbf{A}_{\lambda,t}(0, \dots, 0)$. By arguing as in Section 3.2.2, we can then derive the formulas for calculating transition points of μ_i , and finally the homotopy algorithm for the whole data path, which we summarize in Algorithm 3.

3.2.4 Update from λ_t to λ_{t+1}

Given the previous solution $\mathbf{A}(t, \lambda_t)$, one way to select the hyperparameter value λ is to introduce the empirical objective function [7, 15], which takes the form

$$f_{t+1}(\lambda) = \frac{1}{2} \|\mathbf{x}_{t+1} - \mathbf{A}(t, \lambda) \mathbf{x}_t\|_{\ell_2}^2, \quad (3.17)$$

and to employ the updating rule:

$$\lambda_{t+1} = \lambda_t - \eta \frac{df_{t+1}(\lambda)}{d\lambda} \Big|_{\lambda=\lambda_t}, \quad (3.18)$$

where η is the step size. For convenience, we write $\frac{df_{t+1}(\lambda)}{d\lambda} \Big|_{\lambda=\lambda_t}$ as $\frac{df_{t+1}(\lambda_t)}{d\lambda}$. Analogously, we adopt the notation $\frac{d\mathbf{A}(t, \lambda_t)}{d\lambda}$ to denote the derivative with respect to λ , taken at value $\lambda = \lambda_t$. The objective function f_{t+1} can be interpreted as a one step prediction error on unseen data. Since the Lasso solution is piecewise linear with respect to λ , it follows that when λ is not a transition point, the derivative can be calculated as:

$$\frac{df_{t+1}(\lambda_t)}{d\lambda} = \left\langle \mathbf{G}_t, \frac{d\mathbf{A}(t, \lambda_t)}{d\lambda} \right\rangle = \left\langle \text{Proj}_{\mathcal{G}}(\mathbf{G}_t), \frac{d\mathbf{A}(t, \lambda_t)}{d\lambda} \right\rangle = -\sqrt{2F} \left[\mathbf{a}_1^{\mathbf{G}_t} \right]^\top \left[\mathbf{\Gamma}_0^1 \right]^{-1} \mathbf{w}_1 \quad (3.19)$$

Algorithm 3 Homotopy Algorithm for Data Path

Input: $N, F, \mathbf{\Gamma}_0, \gamma_1, K_N^1, \mathbf{w}_N^1, \lambda, [\mathbf{\Gamma}_0^1]^{-1}, \mathbf{x}_{t+1}, \tilde{\mathbf{X}}_t, t$, where $K_N^1, \mathbf{w}_N^1, [\mathbf{\Gamma}_0^1]^{-1}$ are associated with $\mathbf{A}(t, \frac{t+1}{t}\lambda)$.

Initialization: $K_N^0 \leftarrow K_N \setminus K_N^1, K^1 \leftarrow K \setminus K_N^0$.

for $i = 1, \dots, NF$:

$\mu \leftarrow 0$.

while $\mu < 1$:

Generate \mathbf{w}_1 . $\mathbf{\Gamma}_0^0 = [\mathbf{\Gamma}_0]_{K_N^0, K^1}, \gamma_1^1 = [\gamma_1]_{K^1}, \gamma_1^0 = [\gamma_1]_{K_N^0}$.

$\mathbf{a}_1^s = [\mathbf{\Gamma}_0^1]^{-1} (\gamma_1^1 - (1 + \frac{1}{t})\sqrt{2F}\lambda\mathbf{w}_1), e = \mathbf{x}_{t+1, i} - ([\tilde{\mathbf{X}}_t]_{K^1, i})^\top \mathbf{a}_1^s, \mathbf{u} = [\mathbf{\Gamma}_0^1]^{-1} [\tilde{\mathbf{X}}_t]_{K^1, i},$

8 $\alpha = ([\tilde{\mathbf{X}}_t]_{K^1, i})^\top \mathbf{u}$.

$\mu_k^0 = -t(\mathbf{a}_1^s)_{i(k)} / (\alpha(\mathbf{a}_1^s)_{i(k)} + e(\mathbf{u})_{i(k)}), k \in K_N^1,$

$\mu_k^\pm = \frac{-t(\mathbf{b}^\pm)_{o(k)}}{e(\mathbf{\Gamma}_0^0 \mathbf{u})_{o(k)} - e(\tilde{\mathbf{X}}_t)_{k, i} + \alpha(\mathbf{b}^\pm)_{o(k)}}, k \in K_N^0, \mathbf{b}^\pm = \mathbf{\Gamma}_0^0 \mathbf{a}_1^s - \gamma_1^0 \pm (1 + \frac{1}{t})\sqrt{2F}\lambda,$

$\mu' = \min \{ \min \{ \mu_k^0, k \in K_N^1 : \mu_k^0 > \mu \}, \min \{ \mu_k^+, k \in K_N^0 : \mu_k^+ > \mu \}, \min \{ \mu_k^-, k \in K_N^0 : \mu_k^- > \mu \} \}$.

if $\mu' = \emptyset, \mu' \leftarrow +\infty$.

if $\mu' < 1$:

$\mu = \mu'$.

if μ' is some μ_k^0 :

$K_N^1 \leftarrow K_N^1 \setminus \{k\}, K^1 \leftarrow K^1 \setminus \{k\}, K_N^0 \leftarrow K_N^0 \cup \{k\}$. Remove $(\mathbf{w}_N^1)_{i(k)-d_{DF}}$ from \mathbf{w}_N^1 .

Remove the $i(k)$ -th row, the $i(k)$ -th column from $\mathbf{\Gamma}_0^1$, use block matrix inversion formula to update $[\mathbf{\Gamma}_0^1]^{-1}$.

if μ' is some μ_k^+ (or μ_k^-):

$K_N^0 \leftarrow K_N^0 \setminus \{k\}, K_N^1 \leftarrow K_N^1 \cup \{k\}, K^1 \leftarrow K^1 \cup \{k\}$. Append 1 (or -1) to the end of sign vector \mathbf{w}_N^1 .

Append row $[\mathbf{\Gamma}_0]_{k, K^1}$, column $[\mathbf{\Gamma}_0]_{K^1, k}$ after the last row and last column $\mathbf{\Gamma}_0^1$, respectively,

and use block matrix inversion formula to update $[\mathbf{\Gamma}_0^1]^{-1}$.

else: $\mu = 1$.

23 $[\mathbf{\Gamma}_0^1]^{-1} \xleftarrow{\text{rank 1 update}} [\mathbf{\Gamma}_0^1 + \frac{1}{t}[\tilde{\mathbf{X}}_t]_{K^1, i}([\tilde{\mathbf{X}}_t]_{K^1, i})^\top]^{-1}$

24 $\mathbf{\Gamma}_0 \leftarrow \mathbf{\Gamma}_0 + \frac{1}{t}[\tilde{\mathbf{X}}_t]_{:, i}[\tilde{\mathbf{X}}_t]_{:, i}^\top$

25 $\gamma_1 \leftarrow \gamma_1 + \frac{1}{t}\mathbf{x}_{t+1, i}[\tilde{\mathbf{X}}_t]_{:, i}$

$\mathbf{a}_1^s = \mathbf{a}_1^s + e\mathbf{u}/(t + \alpha)$. Retrieve $\mathbf{A}(t + 1, \lambda)$ based on K^1 and \mathbf{a}_1^s .

$[\mathbf{\Gamma}_0^1]^{-1} \leftarrow \frac{t+1}{t}[\mathbf{\Gamma}_0^1]^{-1}, \mathbf{\Gamma}_0 \leftarrow \frac{t}{t+1}\mathbf{\Gamma}_0, \gamma_1 \leftarrow \frac{t}{t+1}\gamma_1$.

Output: $\mathbf{A}(t + 1, \lambda), K_N^1, \mathbf{w}_N^1, [\mathbf{\Gamma}_0^1]^{-1}, \mathbf{\Gamma}_0, \gamma_1$.

where $\mathbf{a}_1^{\mathbf{G}^t} \in \mathbb{R}^{|K^1|}$ is defined as $(\mathbf{a}_1^{\mathbf{G}^t})_{i(k)} = \langle c_k \mathbf{U}_k, \mathbf{G}_t \rangle, k \in K^1$, with $K^1, \mathbf{w}_1, [\mathbf{\Gamma}_0^1]^{-1}$

associated with $\mathbf{A}(t, \lambda_t)$, and $\mathbf{G}_t = [\mathbf{A}(t, \lambda_t)\mathbf{x}_t - \mathbf{x}_{t+1}]\mathbf{x}_t^\top$. To obtain the non-negative parameter value, we project λ_{t+1} onto interval $[0, +\infty)$ by taking $\max\{\lambda_{t+1}, 0\}$, whenever the result from Equation (3.18) is negative.

Note that λ_{t+1} defined in Equation (3.18) can be interpreted as the online solution from the projected stochastic gradient descent derived for the batch problem, that is,

$$\lambda_n^* = \arg \min_{\lambda \geq 0} \frac{1}{2n} \sum_{t=1}^n \|\mathbf{x}_{t+1} - \mathbf{A}(t, \lambda)\mathbf{x}_t\|_{\ell_2}^2. \quad (3.20)$$

Therefore, the sublinear regret property of projected stochastic gradient descent implies that, when η is given as $\mathcal{O}(\frac{1}{\sqrt{n}})$, we have

$$\frac{1}{2n} \sum_{t=1}^n \|\mathbf{x}_{t+1} - \mathbf{A}(t, \lambda_t)\mathbf{x}_t\|_{\ell_2}^2 - \frac{1}{2n} \sum_{t=1}^n \|\mathbf{x}_{t+1} - \mathbf{A}(t, \lambda_n^*)\mathbf{x}_t\|_{\ell_2}^2 = \mathcal{O}\left(\frac{1}{\sqrt{n}}\right). \quad (3.21)$$

Equation (3.21) implies that in the sense of average one step prediction error defined as Equation (3.20), the adaptive hyperparameter sequence $\{\lambda_t\}_t$ will perform almost as well as the best parameter λ_n^* , for a large number of online updates, with sufficiently small step size η . This completes the online procedure of the second approach, which we conclude in Algorithm 4.

Algorithm 4 Online Structured matrix-variate Lasso

Input: $\mathbf{A}(t, \lambda_t)$, $\mathbf{\Gamma}_0$, γ_1 , K_N^1 , \mathbf{w}_N^1 , λ_t , $[\mathbf{\Gamma}_0^1]^{-1}$, \mathbf{x}_{t+1} , $\tilde{\mathbf{X}}_t$, t , where K_N^1 , \mathbf{w}_N^1 , $[\mathbf{\Gamma}_0^1]^{-1}$ are associated with $\mathbf{A}(t, \lambda_t)$.

Select λ_{t+1} according to Section 3.2.4.

Update $\mathbf{A}(t, \lambda_t) \rightarrow \mathbf{A}(t, \frac{t+1}{t}\lambda_{t+1})$ using Algorithm 2.

Update $\mathbf{A}(t, \frac{t+1}{t}\lambda_{t+1}) \rightarrow \mathbf{A}(t+1, \lambda_{t+1})$ using Algorithm 3.

Output: $\mathbf{A}(t+1, \lambda_{t+1})$, $\mathbf{\Gamma}_0$, γ_1 , K_N^1 , \mathbf{w}_N^1 , λ_{t+1} , $[\mathbf{\Gamma}_0^1]^{-1}$.

4 Augmented Model for Periodic Trends

Up to now, we have discussed methods that are valid for the analysis of stationary time series. For real applications, it is very rare to have stationary time series, thus a *detrend* step is usually performed on raw data before using them in the approaches based on the stationarity assumptions, in order to make the samples closer to the model assumptions.

A common detrend strategy in offline learning is subtracting the sample mean from observations of all time points, that is, given a raw time series $\mathbf{x}_0, \mathbf{x}_1, \dots, \mathbf{x}_t$, we first calculate its sample mean as $\bar{\mathbf{x}}_t = \sum_{\tau=1}^t \mathbf{x}_\tau / t$, then use $\mathbf{x}'_\tau := \mathbf{x}_\tau - \bar{\mathbf{x}}_t$, $\tau = 1, \dots, t$, in the proposed methods. However, this preprocessing strategy is not admissible in the online fashion, since the sample mean changes

every time a new sample comes. Yet, it inspires us to propose the following augmented model of (2.1).

$$\begin{cases} \mathbf{x}_t = \mathbf{b}_t^0 + \mathbf{x}'_t \\ \mathbf{x}'_t = \mathbf{A}\mathbf{x}'_{t-1} + \mathbf{z}_t, \end{cases} \quad (4.1)$$

where $\mathbf{b}_t^0 \in \mathbb{R}^{NF}$, and \mathbf{A} , \mathbf{z}_t are defined in the same way as model (2.1). Model (4.1) is equivalent to model (4.2) below corresponding to another parameterization:

$$\mathbf{x}_t = \mathbf{b}_t + \mathbf{A}\mathbf{x}_{t-1} + \mathbf{z}_t, \quad \mathbf{b}_t = \mathbf{b}_t^0 - \mathbf{A}\mathbf{b}_{t-1}^0. \quad (4.2)$$

The augmented model assumes that the non-stationarity of the observations \mathbf{x}_t is caused by the trend \mathbf{b}_t^0 . We consider in particular, the periodic trend:

$$\mathbf{b}_t^0 = \mathbf{b}_m^0, \quad m = 0, \dots, M-1, \quad m = t \bmod M, \quad (4.3)$$

where M is the length of period. This type of trend is frequently encountered in practice. For example, an annual recurrence ($M = 12$) can be found in many monthly datasets recorded over years. In the following sections, we will adapt the two learning frameworks presented in Section 3 to the augmented model for the periodic trends, and we propose the corresponding algorithms which infer the trends and graphs simultaneously from non-stationary time series \mathbf{x}_t , in an online fashion.

4.1 New OLS Estimators and Asymptotic Distributions

For the augmented model (4.1), we propose a new OLS estimator of \mathbf{A} , which is based on the new estimators of autocovariances, together with the OLS estimator of \mathbf{b}_m^0 . Because two crucial properties to derive the Wald tests in Algorithm 1 are the consistency of sample autocovariances $\hat{\Gamma}_t(0)$, $\hat{\Gamma}_t(1)$, and the CLT of OLS estimator $\check{\mathbf{A}}_t$, we derive the corresponding asymptotic results for the new estimators, and show that these asymptotics are exactly the same as in the stationary case. Therefore, all the results and procedures presented in Section 3.1 can be applied directly on the new estimators. We first define the estimator of \mathbf{A} , still denoted as $\check{\mathbf{A}}_t$, using general least squares (GLS) method:

$$\check{\mathbf{A}}_t, \hat{\mathbf{b}}_{m,t} = \arg \min_{\mathbf{A}, \mathbf{b}_m} \sum_{m=0}^{M-1} S_m(\mathbf{A}, \mathbf{b}_m), \quad (4.4)$$

where $S_m = \sum_{\tau \in I_{m,t}} \tilde{\mathbf{z}}_\tau^\top \Sigma^{-1} \tilde{\mathbf{z}}_\tau$, $\tilde{\mathbf{z}}_\tau = \mathbf{x}_\tau - \mathbf{b}_m - \mathbf{A}\mathbf{x}_{\tau-1}$, with $I_{m,t} = \{\tau = 1, \dots, t : \tau \bmod M = m\}$, and Σ^{-1} the true white noise covariance given in Model (2.1), where $\tilde{\mathbf{z}}_\tau$ represents the residual of the prediction of sample \mathbf{x}_τ . The explicit forms of such minimizers can be found through straightforward calculation, which yields the estimators of autocovariances and trend, denoted as

$\hat{\Gamma}_t(0)$, $\hat{\Gamma}_t(1)$, and $\hat{\mathbf{b}}_{m,t}^0$ respectively, in what follows. More precisely, one has that

$$\begin{cases} \check{\mathbf{A}}_t = \hat{\Gamma}_t(1) \left[\hat{\Gamma}_t(0) \right]^{-1}, \\ \hat{\mathbf{b}}_{m,t} = \bar{\mathbf{x}}_{m,t} - \check{\mathbf{A}}_t \mathbf{x}_{m-1,t}, \quad \hat{\mathbf{b}}_{m,t}^0 = \mathbf{x}_{m,t} \text{ (or } \bar{\mathbf{x}}_{m,t}), \end{cases} \quad (4.5)$$

with

$$\begin{aligned} \hat{\Gamma}_t(0) &= \sum_{m=0}^{M-1} \frac{p_{m,t}}{t} \left(\frac{\sum_{\tau \in I_{m,t}} \mathbf{x}_{\tau-1} \mathbf{x}_{\tau-1}^\top}{p_{m,t}} - \mathbf{x}_{m-1,t} \mathbf{x}_{m-1,t}^\top \right), \quad \hat{\Gamma}_t(1) = \sum_{m=0}^{M-1} \frac{p_{m,t}}{t} \left(\frac{\sum_{\tau \in I_{m,t}} \mathbf{x}_\tau \mathbf{x}_{\tau-1}^\top}{p_{m,t}} - \bar{\mathbf{x}}_{m,t} \mathbf{x}_{m-1,t}^\top \right), \\ p_{m,t} &= |I_{m,t}|, \quad \bar{\mathbf{x}}_{m,t} = \sum_{\tau \in I_{m,t}} \frac{\mathbf{x}_\tau}{p_{m,t}}, \quad m = 0, \dots, M-1, \quad \mathbf{x}_{m-1,t} = \sum_{\tau \in I_{m,t}} \frac{\mathbf{x}_{\tau-1}}{p_{m,t}}, \quad m = 0, \dots, M-1. \end{aligned}$$

To facilitate the notations, in the rest of this paper, we also use $\mathbf{x}_{M-1,t}$ to denote $\mathbf{x}_{-1,t}$, and $p_{m,t}$ to denote the number of times that the samples from the m -th state point in the period have been predicted in the sense of Equation (4.4). As t grows, $\mathbf{x}_{m,t}$ becomes $\bar{\mathbf{x}}_{m,t}$ quickly, for $m = 0, \dots, M-1$, and $p_{m,t}$ becomes $\frac{t}{M}$. For the augmented model, GLS and OLS estimators are still identical, with the latter defined as $\arg \min_{\mathbf{A}, \mathbf{b}_m} \sum_{m=0}^{M-1} \sum_{\tau \in I_{m,t}} \tilde{\mathbf{z}}_\tau^\top \tilde{\mathbf{z}}_\tau$. The estimators given by Formula (4.4) enjoy the asymptotic properties in Proposition (4.1).

Proposition 4.1. *The following asymptotic properties hold for the estimators $\hat{\Gamma}_t(0)$, $\hat{\Gamma}_t(1)$, $\check{\mathbf{A}}_t$, $\hat{\mathbf{b}}_{m,t}^0$, as $t \rightarrow +\infty$,*

- (a) $\hat{\Gamma}_t(0) \xrightarrow{p} \Gamma(0)$, $\hat{\Gamma}_t(1) \xrightarrow{p} \Gamma(1)$,
- (b) $\hat{\mathbf{b}}_{m,t}^0 \xrightarrow{p} \mathbf{b}_m^0$, $\check{\mathbf{A}}_t \xrightarrow{p} \mathbf{A}$,
- (c) $\sqrt{t} \text{vec}(\check{\mathbf{A}}_t - \mathbf{A}) \xrightarrow{d} \mathcal{N}(0, [\Gamma(0)]^{-1} \otimes \Sigma)$,

where $\Gamma(h) = \mathbb{E} \left(\mathbf{x}'_t [\mathbf{x}'_{t-h}]^\top \right)$, $h \geq 0$, $\Sigma = \mathbb{E} (\mathbf{z}_t \mathbf{z}_t^\top)$.

The proofs of the above results are given in Appendix B. Thus, Theorem 3.1 and the bisection Wald test procedure are still valid using $\text{Proj}_{\mathcal{G}_N}(\check{\mathbf{A}}_t)$ and $\hat{\Gamma}_t(0)$, $\hat{\Gamma}_t(1)$ defined in this section. On the other hand, $\hat{\Gamma}_t(0)$ and $\hat{\Gamma}_t(1)$ satisfy the one rank update formulas:

$$\begin{aligned} \hat{\Gamma}_{t+1}(0) &= \frac{t}{t+1} \hat{\Gamma}_t(0) + \frac{1}{t+1} \left[\frac{p_{\bar{m},t}}{p_{\bar{m},t}+1} (\mathbf{x}_t - \mathbf{x}_{\bar{m}-1,t}) (\mathbf{x}_t - \mathbf{x}_{\bar{m}-1,t})^\top \right] \\ \hat{\Gamma}_{t+1}(1) &= \frac{t}{t+1} \hat{\Gamma}_t(1) + \frac{1}{t+1} \left[\frac{p_{\bar{m},t}}{p_{\bar{m},t}+1} (\mathbf{x}_{t+1} - \mathbf{x}_{\bar{m},t}) (\mathbf{x}_t - \mathbf{x}_{\bar{m}-1,t})^\top \right], \end{aligned} \quad (4.6)$$

where $\bar{m} = (t + 1) \bmod M$. Thus, when new sample pair comes, $[\hat{\mathbf{\Gamma}}_{t+1}(0)]^{-1}$ can still be calculated efficiently given the matrix inverse at the previous time. We summarize the extended low dimensional learning framework from model (4.1) in Algorithm 5.

Algorithm 5 Bisection Wald Test for Zero Weights

Input: $\mathbf{x}_{t+1}, \mathbf{x}_t, \hat{\mathbf{\Gamma}}_t(0), \hat{\mathbf{\Gamma}}_t(1), [\hat{\mathbf{\Gamma}}_t(0)]^{-1}, \bar{m}, t, \{p_{m,t}\}_{m=0}^{M-1}, \{\mathbf{x}_{m,t}\}_{m=0}^{M-1}$.

Update $\hat{\mathbf{\Gamma}}_{t+1}(0), \hat{\mathbf{\Gamma}}_{t+1}(1)$ from Equation (4.6).

$$[\hat{\mathbf{\Gamma}}_{t+1}(0)]^{-1} = \frac{t+1}{t} [\hat{\mathbf{\Gamma}}_t(0)]^{-1} - \frac{t+1}{t} \frac{[\hat{\mathbf{\Gamma}}_t(0)]^{-1} (\mathbf{x}_t - \mathbf{x}_{\bar{m}-1,t}) (\mathbf{x}_t - \mathbf{x}_{\bar{m}-1,t})^\top [\hat{\mathbf{\Gamma}}_t(0)]^{-1}}{t(1+p_{\bar{m},t}) + (\mathbf{x}_t - \mathbf{x}_{\bar{m}-1,t})^\top [\hat{\mathbf{\Gamma}}_t(0)]^{-1} (\mathbf{x}_t - \mathbf{x}_{\bar{m}-1,t})},$$

$$\check{\mathbf{A}}_{t+1} = \hat{\mathbf{\Gamma}}_{t+1}(1) [\hat{\mathbf{\Gamma}}_{t+1}(0)]^{-1}.$$

$$\check{\mathbf{\Sigma}}_{t+1} = \hat{\mathbf{\Gamma}}_{t+1}(0) - \hat{\mathbf{\Gamma}}_{t+1}(1) [\hat{\mathbf{\Gamma}}_{t+1}(0)]^{-1} \hat{\mathbf{\Gamma}}_{t+1}(1)^\top.$$

Step *Projection* to *Bisection Wald test procedure* are identical to Algorithm 1.

Let $\hat{\mathbf{A}}_{t+1} = \widehat{\mathbf{A}}_{D,t+1} + \widehat{\mathbf{A}}_{F,t+1} \otimes \widehat{\mathbf{A}}_{N,t+1}$.

Update: $\mathbf{x}_{\bar{m}-1,t+1} \leftarrow \frac{p_{\bar{m},t}}{p_{\bar{m},t}+1} \mathbf{x}_{\bar{m}-1,t} + \frac{1}{p_{\bar{m},t}+1} \mathbf{x}_t$, and $\mathbf{x}_{m,t+1} \leftarrow \mathbf{x}_{m,t}, \forall m \neq \bar{m} - 1$.

$p_{\bar{m},t+1} \leftarrow p_{\bar{m},t} + 1$, and $p_{m,t+1} \leftarrow p_{m,t}, \forall m \neq \bar{m}$,

$t \leftarrow t + 1$.

Output: $\hat{\mathbf{A}}_{t+1}, \hat{\mathbf{\Gamma}}_{t+1}(0), \hat{\mathbf{\Gamma}}_{t+1}(1), [\hat{\mathbf{\Gamma}}_{t+1}(0)]^{-1}, t, \{p_{m,t}\}_{m=0}^{M-1}, \{\mathbf{x}_{m,t}\}_{m=0}^{M-1}$.

4.2 Augmented Structured Matrix-variate Lasso and the Optimality Conditions

To adapt the Lasso-based approach to Model (4.2), the corresponding trend and graph estimators can be obtained by minimizing the augmented Matrix-variate Lasso problem (3.4), which reads as:

$$\mathbf{A}(t, \lambda), \mathbf{b}_m(t, \lambda) = \arg \min_{\mathbf{A} \in \mathcal{K}_G, \mathbf{b}_m} \frac{1}{2t} \sum_{m=0}^{M-1} \sum_{\tau \in I_{m,t}} \|\mathbf{x}_\tau - \mathbf{b}_m - \mathbf{A} \mathbf{x}_{\tau-1}\|_{\ell_2}^2 + \lambda F \|\text{Proj}_{\mathcal{G}_N}(\mathbf{A})\|_{\ell_1}. \quad (4.7)$$

As in the extension of our first approach, the extra bias terms $\mathbf{b}_m, m = 0, \dots, M - 1$, do not affect the core techniques, rather force the methods to consider the M means in the sample autocovariances. Since \mathbf{b}_m only appear in the squares term, the minimizers $\mathbf{b}_m(t, \lambda)$ have the same dependency with $\mathbf{A}(t, \lambda)$ as in Equation (4.5). Thus the trend \mathbf{b}_m^0 can still be estimated by $\mathbf{x}_{m,t}$, and we extend the algorithms in Section 3.2 to update the batch solution of augmented Lasso (4.7) from $\mathbf{A}(t, \lambda_t)$ to $\mathbf{A}(t + 1, \lambda_{t+1})$, given new sample pair $(\mathbf{x}_{t+1}, \mathbf{x}_t)$. To compute the regularization path $\mathbf{A}(t, \lambda_t) \rightarrow \mathbf{A}(t, (1 + \frac{1}{t})\lambda_{t+1})$, Proposition 4.2 implies that Algorithm 2 can still be used, with the adjusted definitions of $\mathbf{\Gamma}_0$ and γ_1 .

Proposition 4.2. *The optimality conditions for $\mathbf{A}(t, \lambda)$ in the matrix-variate Lasso problem*

(4.7) is the following system of equations:

$$\begin{cases} \mathbf{\Gamma}_0^1 \mathbf{a}_1^s - \gamma_1^1 + \sqrt{2F} \lambda \mathbf{w}_1 = 0 \\ \mathbf{\Gamma}_0^0 \mathbf{a}_1^s - \gamma_1^0 + \sqrt{2F} \lambda \mathbf{w}_0 = 0, \end{cases} \quad (4.8)$$

with all variables defined the same way as Proposition 3.2, except that $\hat{\mathbf{\Gamma}}_t(0)$ and $\hat{\mathbf{\Gamma}}_t(1)$ used in these definitions are the sample autovariances of the augmented model, given in Equation (4.5).

For the data path $\mathbf{A}(t, (1 + \frac{1}{t})\lambda_{t+1}) \rightarrow \mathbf{A}(t+1, \lambda_{t+1})$, in the same spirit of Problem (3.13), we introduce variables μ_1, \dots, μ_{NF} to let evolving the matrix-variate Lasso problem (4.7) from time t to $t+1$ through the following variational problem:

$$\begin{aligned} \mathbf{A}_{\lambda_{t+1}, t}(\mu_1, \dots, \mu_{NF}), \mathbf{b}_{m, \lambda_{t+1}, t}(\mu_1, \dots, \mu_{NF}) = & \arg \min_{\mathbf{A} \in \mathcal{K}_G, \mathbf{b}_m} \frac{1}{2(t+1)} \sum_{m=0}^{M-1} \sum_{\tau \in I_{m,t}} \|\mathbf{x}_\tau - \mathbf{b}_m - \mathbf{A} \mathbf{x}_{\tau-1}\|_{\ell_2}^2 \\ & + \frac{1}{2(t+1)} \sum_{i=1}^{NF} \mu_i (\mathbf{x}_{t+1, i} - \mathbf{b}_{\bar{m}, i} - [\mathbf{X}'_t]_{i,:} \text{vec}(\mathbf{A}^0))^2 + \lambda_{t+1} F \|\text{Proj}_{\mathcal{G}_N}(\mathbf{A})\|_{\ell_1}, \end{aligned} \quad (4.9)$$

where $\mathbf{b}_{\bar{m}, i} = (\mathbf{b}_{\bar{m}})_i$, $\bar{m} = (t+1) \bmod M$, and $\mathbf{X}'_t := \sum_{k \in K} \mathbf{U}_k \mathbf{x}_t \text{vec}(\mathbf{U}_k)^\top$. We still denote the objective function in Problem (4.9) by $L_{\lambda_{t+1}, t}(\mu_1, \dots, \mu_{NF})$, and use the notations from Section 3.2.3 here consistently. To extend Algorithm 3, we first calculate the subdifferential of $L_{\lambda_{t+1}, t}(\mu_1, \dots, \mu_{NF})$ at \mathbf{A} , then the optimality conditions follow immediately. To address the structure issue, we always use the constraint-free \mathbf{A}^0 and transfer the structure onto the data vectors. The desired set is given in Proposition 4.3.

Proposition 4.3. *The subdifferential of $L_{\lambda_{t+1}, t}(\mu_1, \dots, \mu_{NF})$ at \mathbf{A}^0 is given by*

$$\begin{aligned} \frac{\partial L_{\lambda_{t+1}, t}(\mu_1, \dots, \mu_{NF})}{\partial \mathbf{A}^0} = & \frac{t}{t+1} \left[\sum_{k, k' \in K} \langle \mathbf{U}_k, \mathbf{U}_{k'} \hat{\mathbf{\Gamma}}_t(0) \rangle \langle \mathbf{U}_{k'}, \mathbf{A}^0 \rangle \mathbf{U}_k - \sum_{k \in K} \langle \mathbf{U}_k, \hat{\mathbf{\Gamma}}_t(1) \rangle \mathbf{U}_k \right] \\ & + \frac{1}{t+1} \sum_{i=1}^{NF} \mu_i \frac{p_{\bar{m}, t}}{p_{\bar{m}, t} + \mu_i} \left[\sum_{k, k' \in K} (\mathbf{x}_t - \mathbf{x}_{\bar{m}-1, t})^\top [\mathbf{U}_k]_{i,:}^\top [\mathbf{U}_{k'}]_{i,:} (\mathbf{x}_t - \mathbf{x}_{\bar{m}-1, t}) \langle \mathbf{U}_{k'}, \mathbf{A}^0 \rangle \mathbf{U}_k \right] \\ & - \frac{1}{t+1} \sum_{i=1}^{NF} \mu_i \frac{p_{\bar{m}, t}}{p_{\bar{m}, t} + \mu_i} \left[\sum_{k \in K} (\mathbf{x}_{t+1, i} - \mathbf{x}_{\bar{m}, t, i}) (\mathbf{x}_t - \mathbf{x}_{\bar{m}-1, t})^\top [\mathbf{U}_k]_{i,:}^\top \mathbf{U}_k \right] \\ & + 2\lambda_{t+1} F \sum_{k \in K_N} \partial |\langle \mathbf{U}_k, \mathbf{A}^0 \rangle| \mathbf{U}_k, \end{aligned} \quad (4.10)$$

where $\hat{\mathbf{\Gamma}}_t(0)$, $\hat{\mathbf{\Gamma}}_t(1)$ are the ones defined in Equation 4.5, and $\mathbf{x}_{\bar{m}, t, i} = (\mathbf{x}_{\bar{m}, t})_i$. Note that, when $(t \bmod M) \neq m$, $\bar{\mathbf{x}}_{m, t} = \mathbf{x}_{m, t}$.

The following remarks can then be made.

Remark 3. *Subdifferential formula (4.10) is almost the same as its stationary counterpart except that the former uses centered data, as well as the appearance of term $\frac{p_{\bar{m},t}}{p_{\bar{m},t}+\mu_i}$.*

Remark 4. *Equation (4.10) implies the update formula (4.6). Since $L_{\lambda_{t+1},t}(1, \dots, 1) = L_{\lambda_{t+1},t+1}$, and $\frac{\partial L_{\lambda_{t+1},t+1}}{\partial \mathbf{A}^0}$ is given in Equation (3.7), with $\lambda = \lambda_{t+1}$, and $\hat{\Gamma}_{t+1}(0)$, $\hat{\Gamma}_{t+1}(1)$ defined the same way as Proposition 4.3. Thus, by equating the quantities in $\langle \mathbf{U}_k, \mathbf{U}_{k'} \cdot \rangle$ and $\langle \mathbf{U}_k, \cdot \rangle$ in the corresponding subdifferential formulas respectively, update formula (4.6) can be induced.*

The optimality conditions of $L_{\lambda_{t+1},t}(\dots, 1, \mu_i, 0, \dots)$ for $\mathbf{A}_{\lambda_{t+1},t}(\dots, 1, \mu_i, 0, \dots)$ have very similar form as Proposition 3.3, except the changes corresponding to Remark 3. We refer Appendix C for the closed-form expression of these specific formulas. Therefore, the derived homotopy algorithm is essentially Algorithm 3 with minor changes, as it can be seen in the corresponding part of Algorithm 6.

Lastly, we derive the updating rule for the regularization parameter. We still consider the one step prediction error, which writes as the following objective function in the case of Model (4.2):

$$f_t(\lambda) = \frac{1}{2} \|\mathbf{x}_{t+1} - \mathbf{b}_{\bar{m}}(t, \lambda) - \mathbf{A}(t, \lambda)\mathbf{x}_t\|_{\ell_2}^2 \quad (4.11)$$

Given the previous solution $\mathbf{A}(t, \lambda_t)$ and $\mathbf{b}_{\bar{m}}(t, \lambda_t)$, we assume that λ_t is not a transition point. Then the derivative of f_t with respect to λ is calculated as:

$$\begin{aligned} \frac{df_t(\lambda_t)}{d\lambda} &= \left\langle \frac{df_t(\lambda)}{d\mathbf{b}_{\bar{m}}(t, \lambda)} \Big|_{\lambda=\lambda_t}, \frac{d\mathbf{b}_{\bar{m}}(t, \lambda_t)}{d\lambda} \right\rangle + \left\langle \frac{df_t(\lambda)}{d\mathbf{A}(t, \lambda)} \Big|_{\lambda=\lambda_t}, \frac{d\mathbf{A}(t, \lambda_t)}{d\lambda} \right\rangle \\ &= \left\langle \mathbf{G}_t^{\mathbf{b}}, -\frac{d\mathbf{A}(t, \lambda_t)}{d\lambda} \mathbf{x}_{\bar{m}-1,t} \right\rangle + \left\langle \mathbf{G}_t, \frac{d\mathbf{A}(t, \lambda_t)}{d\lambda} \right\rangle \\ &= \left\langle [\mathbf{A}(t, \lambda_t)\mathbf{x}_t - \mathbf{x}_{t+1} + \mathbf{b}_{\bar{m}}(t, \lambda_t)][\mathbf{x}_t - \mathbf{x}_{\bar{m}-1,t}]^\top, \frac{d\mathbf{A}(t, \lambda_t)}{d\lambda} \right\rangle \end{aligned} \quad (4.12)$$

where $\mathbf{G}_t^{\mathbf{b}} = \mathbf{b}_{\bar{m}}(t, \lambda_t) - \mathbf{x}_{t+1} + \mathbf{A}(t, \lambda_t)\mathbf{x}_t$, $\mathbf{G}_t = [\mathbf{A}(t, \lambda_t)\mathbf{x}_t - \mathbf{x}_{t+1} + \mathbf{b}_{\bar{m}}(t, \lambda_t)]\mathbf{x}_t^\top$. From Section 3.2.4, $\langle \mathbf{G}_t, \frac{d\mathbf{A}(t, \lambda_t)}{d\lambda} \rangle = -\sqrt{2F} [\mathbf{a}_1^{\mathbf{G}_t}]^\top [\Gamma_0^1]^{-1} \mathbf{w}_1$. The derivatives of the entities of $\mathbf{A}(t, \lambda)$ indexed by K^1 at λ_t can be all found in $\frac{d\mathbf{a}_1(t, \lambda_t)}{d\lambda}$, which equals $-c_k^2 \sqrt{2F} [\Gamma_0^1]^{-1} \mathbf{w}_1$. By contrast, the derivatives of the entities of $\mathbf{A}(t, \lambda)$ indexed by K_N^0 at λ_t all equal zero. Thus, according to the relation of $\mathbf{A}(t, \lambda)$ and \mathbf{a}_1^s defined in Proposition 3.2, matrix $\frac{d\mathbf{A}(t, \lambda_t)}{d\lambda}$ can be constructed. Using the same updating rules of the projected stochastic gradient descent presented in Section 3.2.4, we can compute the online solution λ_{t+1} . We can see that, the introduction of bias terms \mathbf{b}_m into the original models makes them center the raw data automatically during the model fitting. This enables the direct learning over raw time series, while maintaining the performance of methods

comparable to the stationarity-based ones. We summarize the complete learning procedure for the extended Online structured Matrix-variate Lasso in Algorithm 6.

Algorithm 6 Online Structured Matrix-variate Lasso for Graph and Trend Learning

Input: $\mathbf{A}(t, \lambda_t)$, $\mathbf{\Gamma}_0$, γ_1 , K_N^1 , \mathbf{w}_N^1 , λ_t , $[\mathbf{\Gamma}_0^1]^{-1}$, \mathbf{x}_{t+1} , $\tilde{\mathbf{X}}_t$, \bar{m} , t , M , $\{p_{m,t}\}_{m=0}^{M-1}$, $\{\mathbf{x}_{m,t}\}_{m=0}^{M-1}$, $\mathbf{b}_{\bar{m},t}$, where K_N^1 , \mathbf{w}_N^1 , $[\mathbf{\Gamma}_0^1]^{-1}$ are associated with $\mathbf{A}(t, \lambda_t)$.

Select λ_{t+1} according to the end of Section 4.2.

Update $\mathbf{A}(t, \lambda_t) \rightarrow \mathbf{A}(t, \frac{t+1}{t}\lambda_{t+1})$ using algorithm 2.

Center $\mathbf{x}_{t+1} \leftarrow \mathbf{x}_{t+1} - \underline{\mathbf{x}}_{\bar{m},t}$. Compose $\tilde{\mathbf{X}}_{\bar{m}-1,t}$ as $(\tilde{\mathbf{X}}_{\bar{m}-1,t})_{k,i} = c_k[\mathbf{U}_k]_{i;\underline{\mathbf{x}}_{\bar{m}-1,t}}$, and center $\tilde{\mathbf{X}}_t \leftarrow \tilde{\mathbf{X}}_t - \tilde{\mathbf{X}}_{\bar{m}-1,t}$.

Update $\mathbf{A}(t, \frac{t+1}{t}\lambda_{t+1}) \rightarrow \mathbf{A}(t+1, \lambda_{t+1})$ using algorithm 3, with modifications:

Line 8 change to $\alpha = [\tilde{\mathbf{X}}_t]_{K^1,i}^\top \mathbf{u} + p_{\bar{m},t}$,

Line 23, 24, 25 change respectively to:

$$[\mathbf{\Gamma}_0^1]^{-1} \text{rank} \xleftarrow{1 \text{ update}} [\mathbf{\Gamma}_0^1 + \frac{p_{\bar{m},t}}{t(p_{\bar{m},t+1})} [\tilde{\mathbf{X}}_t]_{K^1,i} [\tilde{\mathbf{X}}_t]_{K^1,i}^\top]^{-1}$$

$$\mathbf{\Gamma}_0 \leftarrow \mathbf{\Gamma}_0 + \frac{p_{\bar{m},t}}{t(p_{\bar{m},t+1})} [\tilde{\mathbf{X}}_t]_{:,i} [\tilde{\mathbf{X}}_t]_{:,i}^\top$$

$$\gamma_1 \leftarrow \gamma_1 + \frac{p_{\bar{m},t}}{t(p_{\bar{m},t+1})} \mathbf{x}_{t+1,i} [\tilde{\mathbf{X}}_t]_{:,i}$$

Update $\underline{\mathbf{x}}_{\bar{m}-1,t+1} \leftarrow \frac{p_{\bar{m},t}}{p_{\bar{m},t+1}} \underline{\mathbf{x}}_{\bar{m}-1,t} + \frac{1}{p_{\bar{m},t+1}} \mathbf{x}_t$, and $\underline{\mathbf{x}}_{m,t+1} \leftarrow \underline{\mathbf{x}}_{m,t}, \forall m \neq \bar{m} - 1$.

$p_{\bar{m},t+1} \leftarrow p_{\bar{m},t} + 1$, and $p_{m,t+1} \leftarrow p_{m,t}, \forall m \neq \bar{m}$,

$\bar{m}' \leftarrow (t+2) \bmod M$.

$\mathbf{b}_{\bar{m}',t+1} \leftarrow \underline{\mathbf{x}}_{\bar{m}',t+1} - \mathbf{A}(t+1, \lambda_{t+1}) \underline{\mathbf{x}}_{\bar{m},t+1}$,

$t \leftarrow t + 1$.

Output: $\mathbf{A}(t+1, \lambda_{t+1})$, $\mathbf{\Gamma}_0$, γ_1 , K_N^1 , \mathbf{w}_N^1 , λ_{t+1} , $[\mathbf{\Gamma}_0^1]^{-1}$, t , $\{p_{m,t+1}\}_{m=0}^{M-1}$, $\{\mathbf{x}_{m,t+1}\}_{m=0}^{M-1}$, $\mathbf{b}_{\bar{m}',t+1}$.

5 Experiments

We test the two approaches proposed in Section 3 and their adaptations presented in Section 4 for time series with periodic trends on both synthetic and real dataset. Since the interpretation for the results of both sections are very similar, in this section, we only report the results for the adapted approaches.

5.1 Evaluation procedures on synthetic data

We now present the evaluation procedure for the augmented model approaches. In each simulation, we generate the true graph \mathbf{A} with the structure indicated by \mathcal{K}_G . In particular, we impose sparsity on its sensor graph \mathbf{A}_N by randomly linking a subset of location pairs. The values of non-zero entries in \mathbf{A}_N , and the entries in \mathbf{A}_F , $\text{diag}(\mathbf{A})$ are generated in a random way. Additionally, we generate a trend over a period of M time points for each node and each feature. Therefore true

\mathbf{b}_m^0 , $m = 0, \dots, M - 1$, consists in these NF trend vectors, with each containing M elements. Then, we synthesize very few samples \mathbf{x}_t primarily from Model (4.1) until time t_0 . Figure 1 shows an example of the synthetic time series \mathbf{x}_t , compared with its stationary source \mathbf{x}'_t before adding the periodic trend. The graph and trend estimators proposed in Section 4 only use \mathbf{x}_t . We then set up the batch Lasso problem (4.7) with the generated samples and use its solution $\mathbf{A}(t_0, \lambda_0)$ to start the online procedure of Approach 2 since the next synthetic sample. The batch problem is solved via the accelerated proximal gradient descent with the backtracking line search [16, Section 3.2.2]. We especially set λ_0 as a large number so as to have an over sparse initial solution. Therefore, we expect to see a decreasing λ_t , together with a more accurate estimate $\mathbf{A}(t, \lambda_t)$ as t grows. The updating of $\hat{\mathbf{\Gamma}}_t(0)$ and $\hat{\mathbf{\Gamma}}_t(1)$ starts from $t = 1$, using Formula (4.6), since they are the only inputs of the proximal gradient descent algorithm. However, we wait until there are enough samples for $\hat{\mathbf{\Gamma}}_t(0)$ to be invertible, then we start the online Approach 1 at time t with $[\hat{\mathbf{\Gamma}}_t(0)]^{-1}$. To analyse the performance of the learning approaches, we define the error metrics, average one step prediction error and root mean square deviation (RMSD), respectively in Equations (5.1) and (5.2). We collect the metric values along time.

$$\sum_{\tau=1}^t \frac{\|x_{\tau+1} - \hat{\mathbf{b}}_{m(\tau+1),\tau} - \hat{\mathbf{A}}_{\tau} x_{\tau}\|_2}{t \|x_{\tau+1}\|_2}, \quad m(\tau + 1) = (\tau + 1) \bmod M, \quad (5.1)$$

$$\frac{\|\mathbf{A} - \hat{\mathbf{A}}_t\|_{\mathbf{F}}}{\|\mathbf{A}\|_{\mathbf{F}}}, \quad (5.2)$$

where $\hat{\mathbf{A}}_{\tau}$ denotes the online estimates from the two approaches at time τ , and $\hat{\mathbf{b}}_{m,\tau} = \mathbf{x}_{m,\tau} - \check{\mathbf{A}}_{\tau} \mathbf{x}_{m-1,\tau}$ for Approach 1, while $\hat{\mathbf{b}}_{m,\tau} = \mathbf{x}_{m,\tau} - \mathbf{A}(\tau, \lambda_{\tau}) \mathbf{x}_{m-1,\tau}$ for Approach 2. We perform such simulation multiple times to obtain furthermore the means and the standard deviations of error metrics at each iteration (when the estimators are available) to better demonstrate the performance. The true graph \mathbf{A} and trends \mathbf{b}_m^0 are generated independently across these simulations.

5.2 Simulation results

We firstly visualize the representative estimates in heatmap with $N = 10$, $F = 4$, and $M = 12$ for illustration purpose. Then we plot the evolution of error metrics, regularization parameter of 30 simulations for $N = 20$, $F = 5$, and $M = 12$. Lastly, we report the running time. The hyperparameter settings are given in the captions of figures of corresponding results.

Figures 2, 3 show the estimated graphs of two approaches when their corresponding online procedures start. In Figure 2, we can see that the batch solution which starts Approach 2 is over sparse due to the large λ_0 . We can notice from Figure 3 that, the two initial estimations of $\mathbf{A}_{\mathbf{F}}$ are already satisfactory, especially the Lasso solution which uses only 20 samples. Actually, estimations of $\mathbf{A}_{\mathbf{F}}$ and $\text{diag}(\mathbf{A})$ converge to the truth very quickly in both case when N is

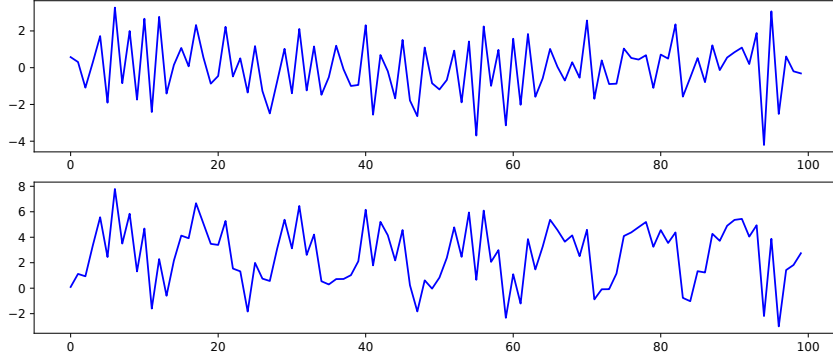


Figure 1: Top is the stationary time series from Model (2.2) at one component, bottom is the above time series with added periodic trend ($M = 12$).

significantly larger than F . Figures 4 and 5 show that the graph estimators of both approaches tend to the true graph as more samples are received. Meanwhile, Figure 6 shows the effectiveness of trend estimator $\underline{\mathbf{x}}_{m,t}$ defined in Equation (4.5).

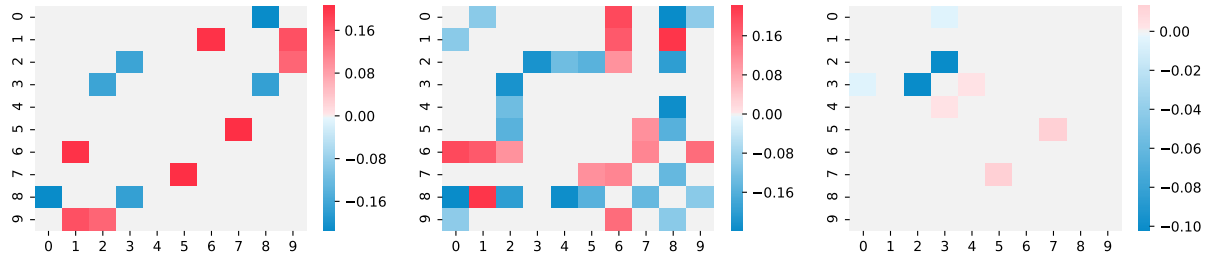


Figure 2: *Initial sensor graph estimates which start the online procedures.* True \mathbf{A}_N (left), $\widehat{\mathbf{A}}_{N,91}$ of Approach 1 (middle), and $\mathbf{A}_N(20,0.05)$ of Approach 2 (right) are represented by heatmaps. Simulation settings: $N = 10$, $F = 4$, number of model parameters = 571, significance level of χ^2 test = 0.1.

We now show the numeric results of 30 simulations, with $N = 20$, $F = 5$, and $M = 12$. We test three different step size η , 5×10^{-7} , 1×10^{-6} , and 5×10^{-6} . With each value we perform 10 independent simulations. Figure 7, 8 plot the evolution of error metrics (5.1) and (5.2), respectively. For better visualization effect, since the performance of Approach 1 does not depend on η , we only show one mean metric curve instead of 3, in the two figures, which is calculated from the results of these 30 simulations.

Figures 7, 8 show the convergence of graph estimators of both approaches, moreover, for

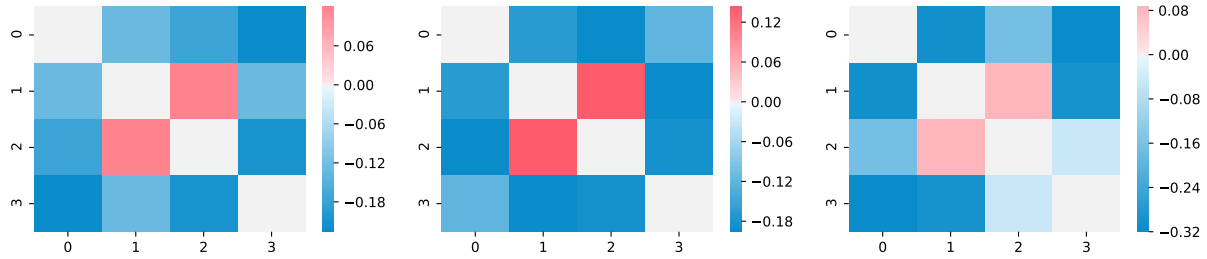


Figure 3: *Initial feature graph estimates which start the online procedures.* True \mathbf{A}_F (left), $\widehat{\mathbf{A}}_{F,91}$ of Approach 1 (middle), and $\mathbf{A}_F(20, 0.05)$ of Approach 2 (right). Simulation settings: $N = 10$, $F = 4$, number of model parameters = 571.

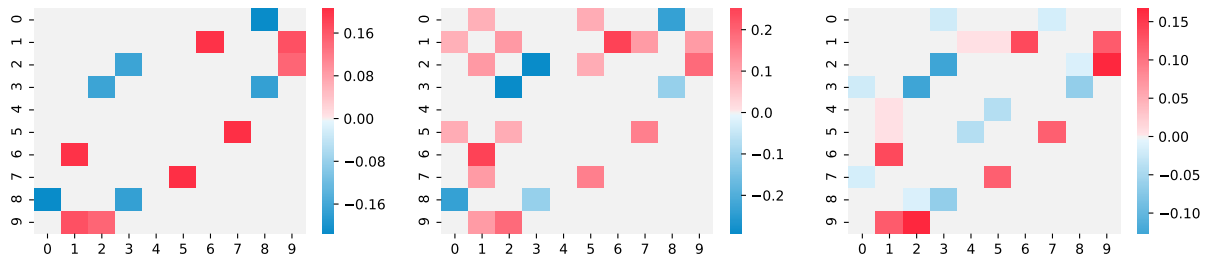


Figure 4: *Sensor graph estimated at the arrival of the 182-th sample.* True \mathbf{A}_N (left), $\widehat{\mathbf{A}}_{N,182}$ of Approach 1 (middle), and $\mathbf{A}_N(182, 0.0286)$ of Approach 2 (right) are represented by heatmaps. Simulation settings: $N = 10$, $F = 4$, number of model parameters = 105, significance level of χ^2 test = 0.1, $\eta = 5 \times 10^{-6}$.

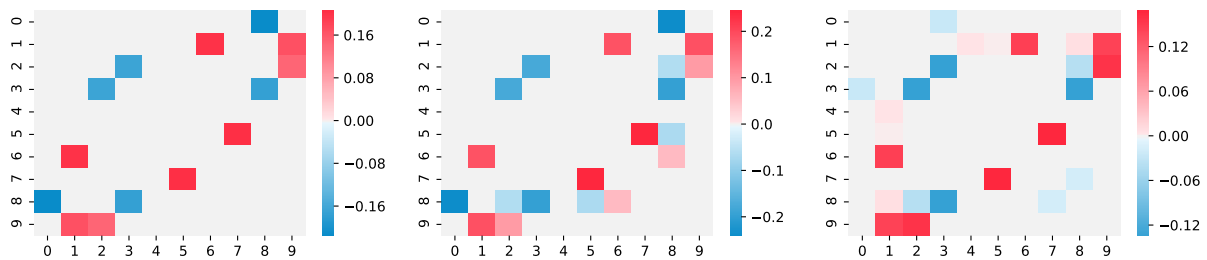


Figure 5: *Sensor graph estimated at the arrival of the 591-th sample.* True \mathbf{A}_N (left), $\widehat{\mathbf{A}}_{N,591}$ of Approach 1 (middle), and $\mathbf{A}_N(591, 0.0130)$ of Approach 2 (right) are represented by heatmaps. Simulation settings: $N = 10$, $F = 4$, number of model parameters = 571, significance level of χ^2 test = 0.1, $\eta = 5 \times 10^{-6}$.

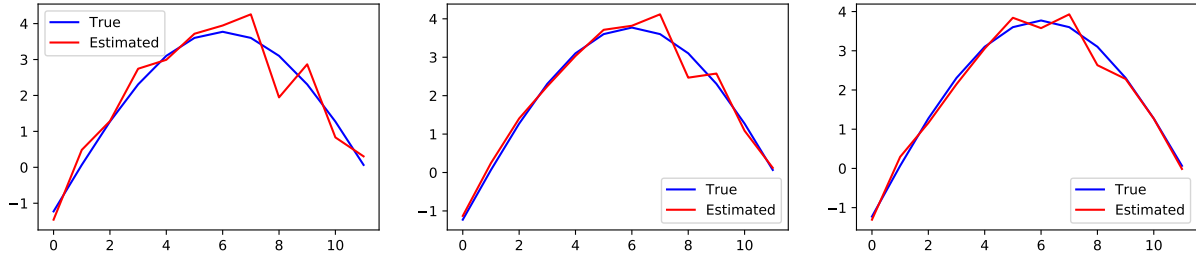


Figure 6: *Trend of the first sensor, first feature, estimated at different time.* Estimation at $t = 182$ (left), $t = 273$ (middle), $t = 591$ (right). Simulation settings: $N = 10$, $F = 4$, $M = 12$, number of model parameters = 571.

Approach 2, the step sizes η determines the convergence speed. Especially, we can see from Figure 7 that the RMSD of Approach 2 with $\eta = 5 \times 10^{-6}$ decreases the most quickly for the first 100 iterations, after which it starts to slow down and decrease more slowly than the RMSDs of the other two step sizes. For Approach 1, when its estimator is available in the high-dimensional phase, the RMSD decreases very fast, and it shows the trend to keep decreasing for larger sample size. Nevertheless, the estimator of Approach 1 performs worse than the Lasso estimators in the sense of the prediction of unseen data, as shown in Figure 8. This is likely linked with the fact that, the selection procedure updates the regularization parameter of Lasso estimator towards the direction which minimizes the one step prediction error (5.1). For synthetic data, it is not surprising that the RMSD from Approach 1 will eventually become zero, because these data are precisely sampled from the model used in the method derivation. On the other hand, at each online iteration, the OLS estimation is calculated accurately. By contrast, for the homotopy algorithms, they still introduce small errors, possibly due to the following assumptions used in the derivation of the method: 1. the active elements of K_N^1 of the algorithm inputs are not zero³; 2. the sub-derivatives of those zero elements are strictly within $(-1, 1)$; 3. every λ_t at which we calculate the derivative as in Section 3.2.4 are not a transition point. Thus, for example, small non-zero element values in the inputs may cause the numerical errors. However, in real applications, the only available metric which allows the performance comparison is the prediction error (5.1).

Figure 9 demonstrates the performance of the updating method of the regularizing parameter λ , and the impact from different step size values η . The curves emphasize the convergence of the estimation updated by online Approach 2. Moreover, we can observe that λ_t are decreasing, which was expected at the experiment design. On the other hand, the results show that a larger step size will make the convergence faster, yet more affected by the noise, especially when the

³This hypothesis means that, some zero $(\mathbf{a}_1^s)_{i(k)}$, $k \in K_N^1$ should not satisfy the first equations of the optimality condition (3.8) and (3.14), due to the computation coincidence.

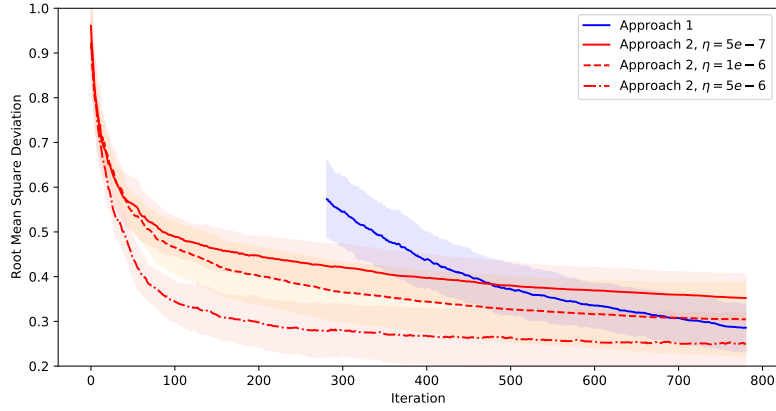


Figure 7: *Root mean square deviation.* The red curves are the mean RMSD of Approach 2, taken over 10 simulations each. The blue curve is the mean RMSD of Approach 1, taken over the same 30 simulations. The shaded areas represent the corresponding one standard deviations. Other simulation settings: $N = 20$, $F = 5$, $M = 12$, number of model parameters = 1500, significance level of χ^2 test = 0.1, $t_0 = 20$, $\lambda_0 = 0.03$. In the first low dimensional phase, the accurate estimator of Approach 1 is not available.

solution is converged.

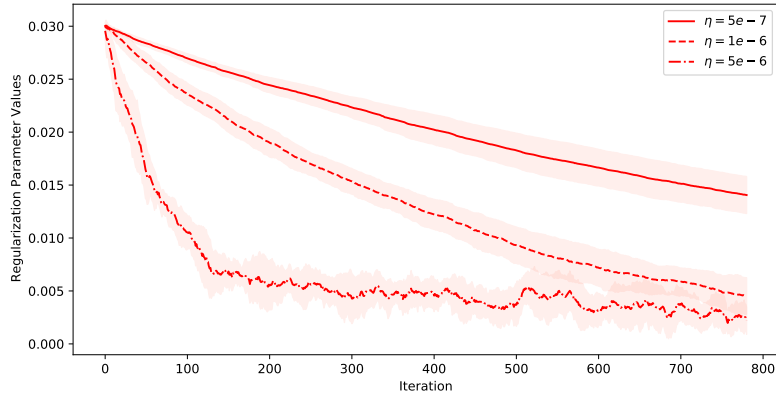


Figure 9: *Regularization parameter evolution.* The red curves are the mean regularization parameter values, taken over 10 simulations each. The shaded areas represent the corresponding one standard deviations. Other simulation settings: $N = 20$, $F = 5$, $M = 12$, number of model parameters = 1500, $t_0 = 20$, $\lambda_0 = 0.03$.

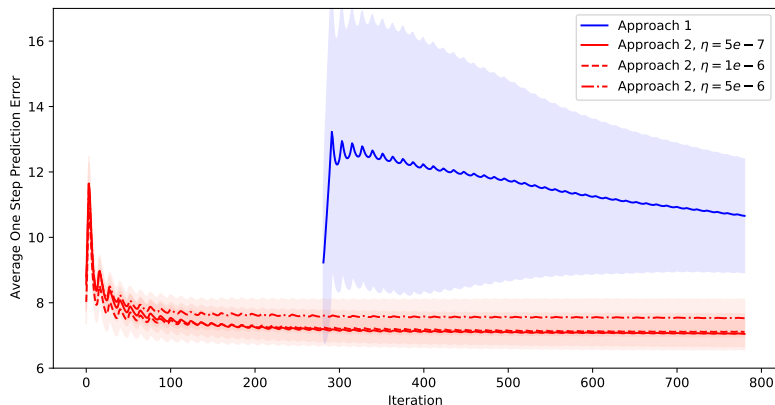


Figure 8: *Average one step prediction error.* The red curves are the mean prediction error of Approach 2, taken over 10 simulations each. The blue curve is the mean prediction error of Approach 1, taken over the same 30 simulations. The shaded areas represent the corresponding one standard deviations. Other simulation settings: $N = 20$, $F = 5$, $M = 12$, number of model parameters = 1500, significance level of χ^2 test = 0.1, $t_0 = 20$, $\lambda_0 = 0.03$.

We also compare the running time of a single online update for the two methods in Figure 10. Firstly, it is clear that updating the Lasso solutions by the homotopy algorithms saves considerable time, which is on average 0.20 seconds for the graph size $N = 20$, $F = 5$. The running time of the accelerated proximal gradient descent performed in the beginning of these simulations costs more than 3 seconds. By contrast, an update using Approach 1 takes 25 seconds on average. We can also notice that Approach 1 with larger step size runs slower, because the updated regularization parameter is more different than the preceding one, as explained by the results in Figure 9.

Lastly, it is worth to point that because the true \mathbf{A}_N has high level of sparsity, thus with lower significance level, Wald test will accept $H_0 : \alpha = 0$ more easily, and we can observe the Wald estimator $\widehat{\mathbf{A}}_{N,t}$ rejects those false non-zero entries faster. Nevertheless, since for real data, we do not know the true graph sparsity, thus the significance level can be regarded as the hyperparameter which controls the desired sparsity as well for the first approach.

5.3 Climatology Data

We use the U.S. Historical Climatology Network (USHCN) data⁴ to test our proposed approaches. The dataset contains monthly averages of four climatology measurements, recorded at the weather stations located across the United States, over years of period. The four measurements are: minimal temperature, maximal temperature, mean temperature, and precipitation. Figure 11 is a

⁴The dataset is available at <https://www.ncdc.noaa.gov/ushcn/data-access>

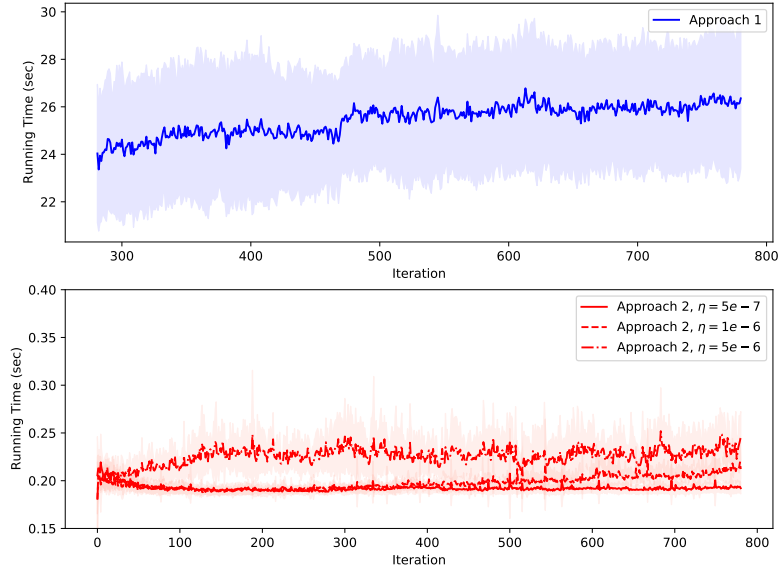


Figure 10: *Running time of each online update.* The red curves are the mean running time of Approach 2, taken over 10 simulations each. The blue curve is the mean running time of Approach 1, taken over the same 30 simulations. The shaded areas represent the corresponding one standard deviations. Other simulation settings: $N = 20$, $F = 5$, $M = 12$, number of model parameters = 1500, significance level of χ^2 test = 0.1, $t_0 = 20$, $\lambda_0 = 0.03$.

snippet of the dataset, which illustrates these measurement time series observed from a certain spatial location. A clear periodic trend can be seen from each univariate time series, with period length equal 12 months. We can also notice that some observations are missing in the dataset, to focus on the evaluation of learning approaches, we do not consider the stations with incomplete time series. Geographically, we picked data only from the California and Nevada states for this experiment. The summary of experiment setting thus is: $N = 27$, $F = 4$, $M = 12$, total number of time points = 1523 months (cover the years from 1894 to 2020). We apply the approaches from Section 4 on the raw time series to learn the weather graph of the region. The testing procedure using the real data is identical to the evaluation procedure with the synthetic data. We use the first $t_0 + 1$ observations to set up the corresponding batch Lasso problem, and use its solution to start Approach 2. Approach 1 will be started once $\hat{\mathbf{\Gamma}}_t(0)$ become invertible. The average one step prediction error is calculated along online iterations. t_0 and λ_0 are always set as 20 and 0.03, respectively, whose values do not affect the methods' performance much, because of the adaptive tuning procedures of the regularization parameter.

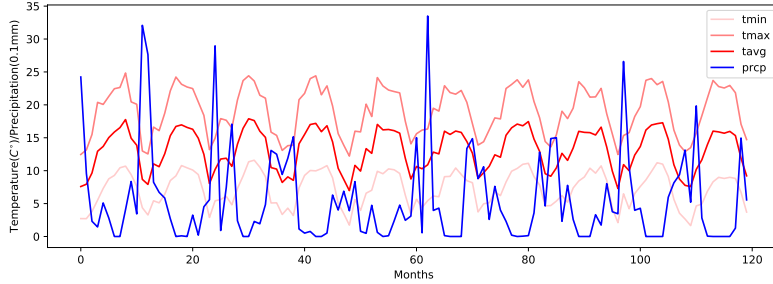


Figure 11: *Learning set for augmented model based approaches.* Monthly records of minimal temperature, maximal temperature, mean temperature, and precipitation from Station USH00040693 over a period over 20 years.

5.4 Online Graph Learning with Raw Time Series

Figure 12, 13 show the sensor graphs learned by the two proposed approaches in Section 4 updated at different time. Figure 14 plots the evolution of regularization parameter value. We can see that, for Approach 2, when more observations are received, it considers more location pairs actually Granger-cause each other. On the other hand, compared to the estimated graphs from Approach 2, those from Approach 1 vary more along time, which can be caused by the facts: 1. in the early stage, $\hat{\Gamma}_t(0)$ is still ill-conditioned, therefore its inverse brings unstable OLS solutions; 2. Approach 1 relies on large sample properties of the designed estimators. These points are also supported by the average one step prediction curve given in Figure 15, where it is shown that, the prediction error of Approach 1 is significantly larger than Approach 2, especially when sample size is around 500 to 800.

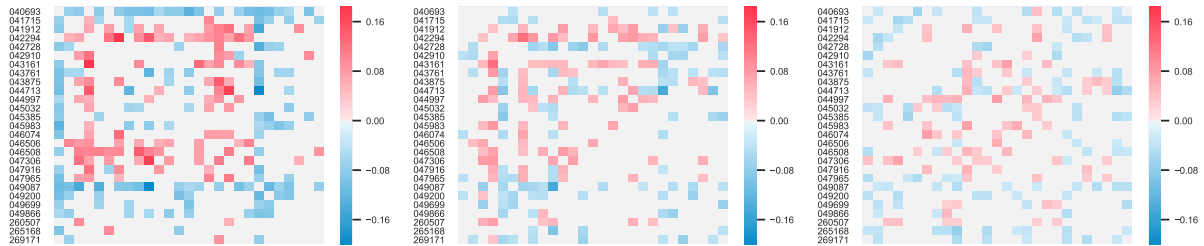


Figure 12: *Updated sensor graph by Approach 1 at different time.* $t = 507$ (left), $t = 1015$ (middle), and $t = 1522$ (right). Experiment settings: $N = 27$, $F = 4$, $M = 12$, number of model parameters = 1761, significance level of χ^2 test = 0.1, $\eta = 10^{-5}$, $t_0 = 20$, $\lambda_0 = 0.03$. The row labels are the 6-digit Cooperative Observer Identification Number of the corresponding weather stations.

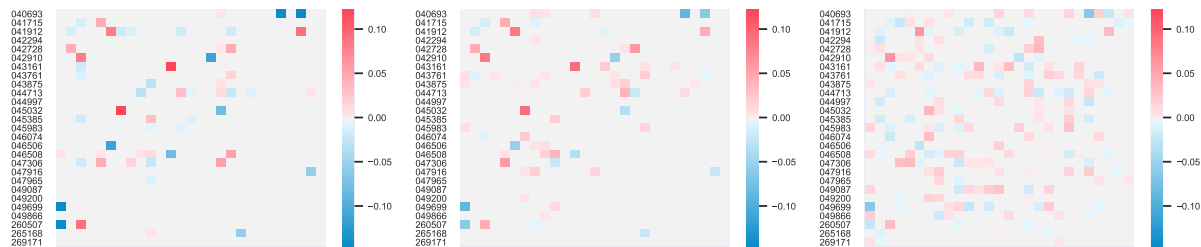


Figure 13: *Updated sensor graph by Approach 2 at different time.* $t = 507$ (left), $t = 1015$ (middle), and $t = 1522$ (right). Experiment settings: $N = 27$, $F = 4$, $M = 12$, number of model parameters = 1761, significance level of χ^2 test = 0.1, $\eta = 10^{-5}$, $t_0 = 20$, $\lambda_0 = 0.03$. The rows and columns correspond to the weather stations whose 6-digit Cooperative Observer Identification Number are given by the row labels.

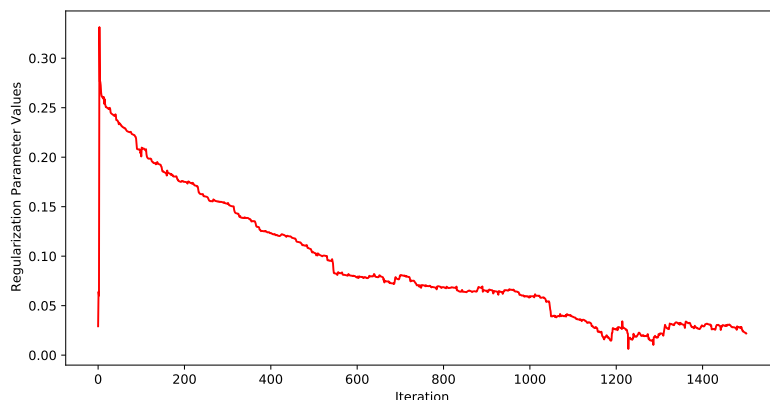


Figure 14: *Regularization parameter evolution.* Experiment settings: $N = 27$, $F = 4$, $M = 12$, number of model parameters = 1761, significance level of χ^2 test = 0.1, $\eta = 10^{-5}$, $t_0 = 20$, $\lambda_0 = 0.03$.

Next we show the last updated feature graphs in Figure 16. We can see that the estimated measurement relationship from the two approaches coincide in t_{\min} and t_{\max} , t_{\min} and t_{avg} , t_{\min} and prcp . However, the relationship between t_{avg} and prcp is very weak in the Lasso estimator, while strong in the projected OLS estimator.

In particular, Figure 17 reports the evolution of estimated trends from one representative spatial location along time, where we can clearly observe the increase of temperature from the past to the present.

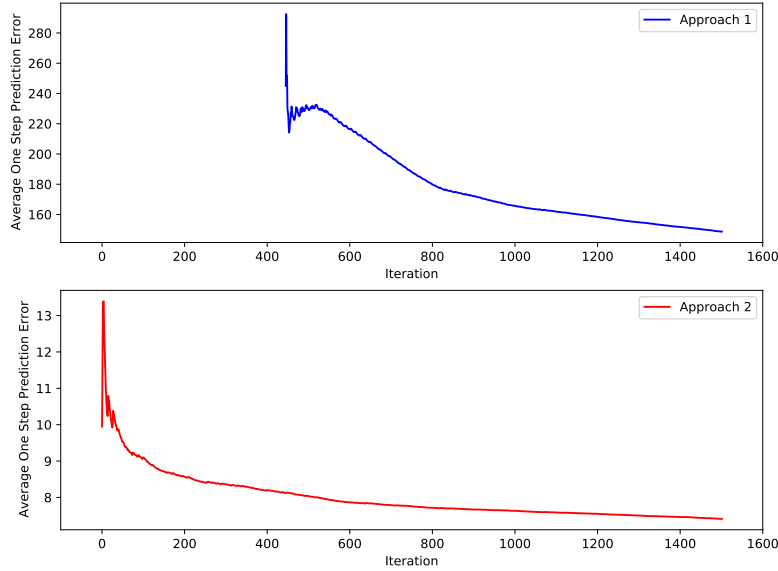


Figure 15: *Average one step prediction error of raw time series.* Approach 1 (top), and Approach 2 (bottom).



Figure 16: *Updated feature graph at $t = 1522$.* Approach 1 (left), and Approach 2 (right). Experiment settings: $N = 27$, $F = 4$, $M = 12$, number of model parameters = 1761, significance level of χ^2 test = 0.1, $\eta = 10^{-5}$, $t_0 = 20$, $\lambda_0 = 0.03$.

Lastly, in Figure 18, we plot the edge overlap (considering the signs of weights) of the two last updated sensor graphs, furthermore, visualize this overlap sensor graph on the actual geographical graph. We can see that the remote weather stations have less dependency with other stations, while more edges appear within the area where lots of stations are densely located together. These observations imply that the inferred graphs provide the consistent weather patterns with

geographical features. Furthermore, they validate the legitimacy of model assumptions (2.1) and (4.1), as well as the effectiveness of the proposed learning methods.

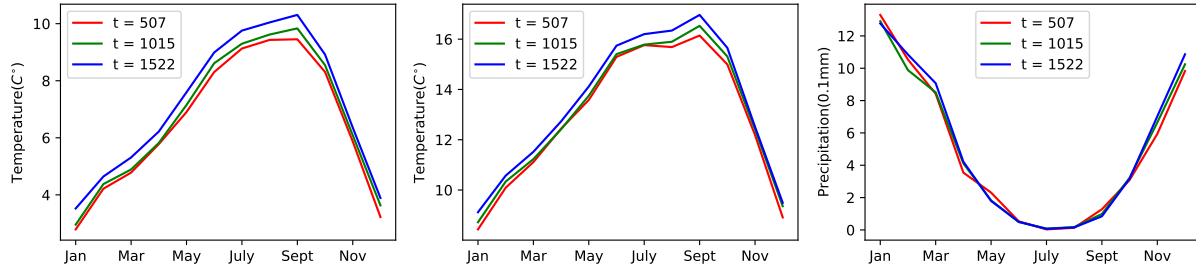


Figure 17: *Estimated trends along years.* On the left, middle, right are the estimated trends at different years of Station USH00040693 for minimal temperature, average temperature, and precipitation respectively. Experiment settings: $N = 27$, $F = 4$, $M = 12$.

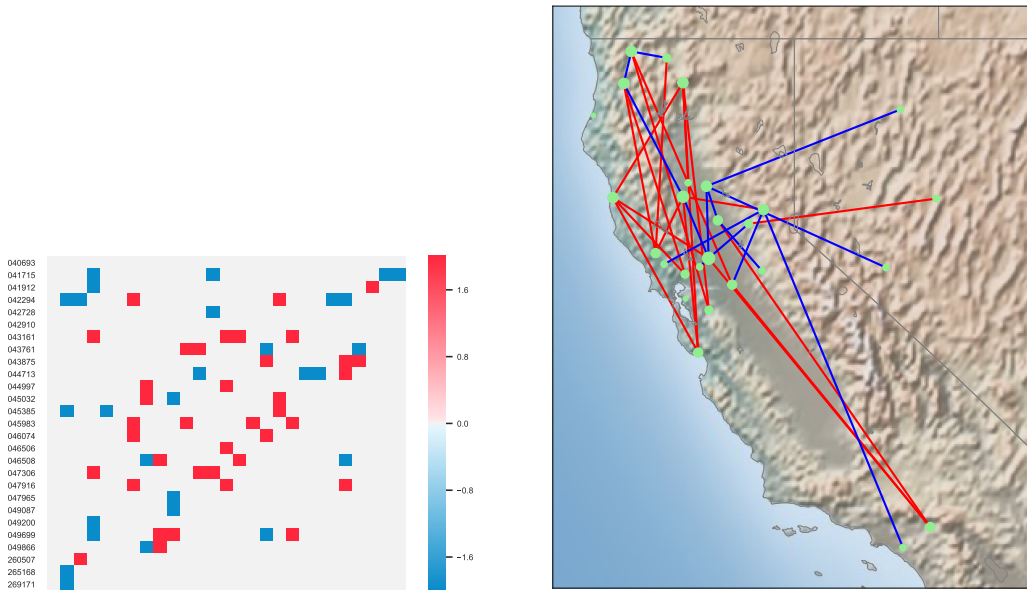


Figure 18: *Overlap sensor graph.* On the left is the adjacency matrix of an unweighed undirected graph which is the overlap of the two last updated sensor graphs in Figure 13, with the colors reporting the common edge signs. On the right is the visualization of this overlap sensor graph on the actually geographical map. The nodes with bigger sizes connect with more nodes.

6 Conclusion

In this paper, we firstly derived two learning frameworks for inferring the proposed structured VAR model in an online fashion. Then, we proposed the augmented data model for the matrix-variate time series with periodic trends, and extended both learning frameworks for the inference of augmented model to update the estimated graph and trends simultaneously. These frameworks provide useful techniques to address the structure constraint in low and high dimensional regime respectively. Especially for high-dimensional regime, we introduced a novel Lasso-type problem (3.4), for which we extended the Homotopy algorithms of standard Lasso. Lasso (3.4) differs from standard Lasso (3.5) not only by replacing the coefficient vector with the coefficient matrix \mathbf{A} , but mainly by requiring \mathbf{A} to have the desired structure indicated by \mathcal{K} and the partial sparsity penalized by $\|\text{Proj}_{\mathcal{G}_N}(\mathbf{A})\|_{\ell_1}$. Notice that the derivations of all the proposed algorithms do not rely on the specific structure constraint, nor on the particular partial sparsity regularization. Therefore, they can be easily adapted to other model designs. Other model extensions are possible, for example, from matrix-variate to tensor-variate time series by using the multi-way Kronecker sum notion, or considering more time lag terms in VAR model, and accordingly replacing Lasso penalty with group Lasso penalty in (3.4). We tested our approaches using both synthetic and real data, and observed very promising results.

References

- [1] Bach, F. R. and Jordan, M. I. Learning graphical models for stationary time series. *IEEE transactions on signal processing*, 52(8):2189–2199, 2004.
- [2] Bolstad, A., Van Veen, B. D., and Nowak, R. Causal network inference via group sparse regularization. *IEEE transactions on signal processing*, 59(6):2628–2641, 2011.
- [3] Dong, X., Thanou, D., Frossard, P., and Vandergheynst, P. Learning laplacian matrix in smooth graph signal representations. *IEEE Transactions on Signal Processing*, 64(23):6160–6173, 2016.
- [4] Dong, X., Thanou, D., Rabbat, M., and Frossard, P. Learning graphs from data: A signal representation perspective. *IEEE Signal Processing Magazine*, 36(3):44–63, 2019.
- [5] Efron, B., Hastie, T., Johnstone, I., Tibshirani, R., et al. Least angle regression. *Annals of statistics*, 32(2):407–499, 2004.
- [6] Friedman, J., Hastie, T., and Tibshirani, R. Sparse inverse covariance estimation with the graphical lasso. *Biostatistics*, 9(3):432–441, 2008.
- [7] Garrigues, P. and Ghaoui, L. An homotopy algorithm for the lasso with online observations. *Advances in neural information processing systems*, 21:489–496, 2008.

- [8] Greenewald, K., Zhou, S., and Hero III, A. Tensor graphical lasso (teralasso). *Journal of the Royal Statistical Society: Series B (Statistical Methodology)*, 81(5):901–931, 2019.
- [9] Kalaitzis, A., Lafferty, J., Lawrence, N. D., and Zhou, S. The bigraphical lasso. In *International Conference on Machine Learning*, pp. 1229–1237. PMLR, 2013.
- [10] Kalofolias, V. How to learn a graph from smooth signals. In *Artificial Intelligence and Statistics*, pp. 920–929. PMLR, 2016.
- [11] Lütkepohl, H. *New introduction to multiple time series analysis*. Springer Science & Business Media, 2005.
- [12] Malioutov, D. M., Cetin, M., and Willsky, A. S. Homotopy continuation for sparse signal representation. In *Proceedings.(ICASSP'05). IEEE International Conference on Acoustics, Speech, and Signal Processing, 2005.*, volume 5, pp. v–733. IEEE, 2005.
- [13] Mei, J. and Moura, J. M. Signal processing on graphs: Causal modeling of unstructured data. *IEEE Transactions on Signal Processing*, 65(8):2077–2092, 2016.
- [14] Meinshausen, N., Bühlmann, P., et al. High-dimensional graphs and variable selection with the lasso. *Annals of statistics*, 34(3):1436–1462, 2006.
- [15] Monti, R. P., Anagnostopoulos, C., and Montana, G. Adaptive regularization for lasso models in the context of nonstationary data streams. *Statistical Analysis and Data Mining: The ASA Data Science Journal*, 11(5):237–247, 2018.
- [16] Parikh, N. and Boyd, S. Proximal algorithms. *Foundations and Trends in optimization*, 1(3): 127–239, 2014.
- [17] Sandryhaila, A. and Moura, J. M. Big data analysis with signal processing on graphs: Representation and processing of massive data sets with irregular structure. *IEEE Signal Processing Magazine*, 31(5):80–90, 2014.
- [18] Songsiri, J. and Vandenberghe, L. Topology selection in graphical models of autoregressive processes. *The Journal of Machine Learning Research*, 11:2671–2705, 2010.
- [19] Wang, Y., Jang, B., and Hero, A. The sylvester graphical lasso (syglasso). In *International Conference on Artificial Intelligence and Statistics*, pp. 1943–1953. PMLR, 2020.

A Proof of Results in Section 3.1 and the CLT for $\widehat{\mathbf{A}}_t$

Proof of Theorem 3.1. By Cramér-Wold theorem, (b) $\sqrt{t} \text{vec}(\check{\mathbf{A}}_t - \mathbf{A}) \xrightarrow{d} \mathcal{N}(0, \boldsymbol{\Sigma}_{ols})$ is equivalent to:

$$\langle \boldsymbol{\Lambda}, \sqrt{t} (\check{\mathbf{A}}_t - \mathbf{A}) \rangle \xrightarrow{d} \mathcal{N}(0, \text{vec}(\boldsymbol{\Lambda})^\top \boldsymbol{\Sigma}_{ols} \text{vec}(\boldsymbol{\Lambda})) \quad (\text{A.1})$$

holds for all $\boldsymbol{\Lambda} \in \mathbb{R}^{NF \times NF}$. On the other hand, we can express any entity of $\widehat{\mathbf{A}}_{N,t}$ as a linear function of $\check{\mathbf{A}}_t$:

$$\widehat{\mathbf{A}}_{N,t} = \sum_{1 \leq l < h \leq N} \langle c_N^2 \mathbf{I}_F \otimes (\mathbf{u}_l \mathbf{u}_h^\top + \mathbf{u}_h \mathbf{u}_l^\top), \check{\mathbf{A}}_t \rangle (\mathbf{u}_l \mathbf{u}_h^\top + \mathbf{u}_h \mathbf{u}_l^\top). \quad (\text{A.2})$$

Thus, $\text{svec} \left(\sqrt{t} (\widehat{\mathbf{A}}_N - \mathbf{A}_N) \right) = \sum_{1 \leq l < h \leq N} \langle c_N^2 \mathbf{I}_F \otimes (\mathbf{u}_l \mathbf{u}_h^\top + \mathbf{u}_h \mathbf{u}_l^\top), \sqrt{t} (\check{\mathbf{A}}_t - \mathbf{A}) \rangle \text{svec}(\mathbf{u}_l \mathbf{u}_h^\top)$. Then for all $\lambda \in \mathbb{R}^{\frac{N(N-1)}{2}}$, we have

$$\begin{aligned} & \lambda^\top \text{svec} \left(\sqrt{t} (\widehat{\mathbf{A}}_N - \mathbf{A}_N) \right) \\ &= \left\langle \sum_{1 \leq l < h \leq N} c_N^2 \lambda^\top \text{svec}(\mathbf{u}_l \mathbf{u}_h^\top) \mathbf{I}_F \otimes (\mathbf{u}_l \mathbf{u}_h^\top + \mathbf{u}_h \mathbf{u}_l^\top), \sqrt{t} (\check{\mathbf{A}}_t - \mathbf{A}) \right\rangle. \end{aligned}$$

Let $\boldsymbol{\Lambda}$ in Equation (A.1) be

$$\sum_{1 \leq l < h \leq N} c_N^2 \lambda^\top \text{svec}(\mathbf{u}_l \mathbf{u}_h^\top) \mathbf{I}_F \otimes (\mathbf{u}_l \mathbf{u}_h^\top + \mathbf{u}_h \mathbf{u}_l^\top),$$

then we have

$$\lambda^\top \text{svec} \left(\sqrt{t} (\widehat{\mathbf{A}}_{N,t} - \mathbf{A}_N) \right) \xrightarrow{d} \mathcal{N}(0, \text{vec}(\boldsymbol{\Lambda})^\top \boldsymbol{\Sigma}_{ols} \text{vec}(\boldsymbol{\Lambda})).$$

Notice that, $\text{vec}(\boldsymbol{\Lambda}) = \lambda^\top \sum_{1 \leq l < h \leq N} c_N^2 \text{svec}(\mathbf{u}_l \mathbf{u}_h^\top) \tilde{\mathbf{u}}_{lh}$. Thus $\text{vec}(\boldsymbol{\Lambda})^\top \boldsymbol{\Sigma}_{ols} \text{vec}(\boldsymbol{\Lambda}) = \lambda^\top \boldsymbol{\Sigma}_N \lambda$. Use Cramér-Wold theorem again, we can get the theorem result. ■

Theorem A.1. (CLT for $\widehat{\mathbf{A}}_t$)

$$\sqrt{t} \text{vec}(\widehat{\mathbf{A}}_t - \mathbf{A}) \xrightarrow{d} \mathcal{N}(0, \boldsymbol{\Sigma}_G) \quad (\text{A.3})$$

where $\boldsymbol{\Sigma}_G = \sum_{k, k' \in K} \text{vec}(\mathbf{U}_k)^\top \boldsymbol{\Sigma}_{ols} \text{vec}(\mathbf{U}_{k'}) [\text{vec}(\mathbf{U}_k) \text{vec}(\mathbf{U}_{k'})^\top]$.

Proof: The proof is similar as before. Because, we can express any entity of $\widehat{\mathbf{A}}_t$ as a linear function of $\check{\mathbf{A}}_t$:

$$\widehat{\mathbf{A}}_t = \sum_{k \in K} \langle \mathbf{U}_k, \check{\mathbf{A}}_t \rangle \mathbf{U}_k. \quad (\text{A.4})$$

Thus, for all $\mathbf{\Lambda}' \in \mathbb{R}^{NF \times NF}$, we have

$$\langle \mathbf{\Lambda}', \sqrt{t} (\widehat{\mathbf{A}}_t - \mathbf{A}) \rangle = \left\langle \sum_{k \in K} \langle \mathbf{\Lambda}', \mathbf{U}_k \rangle \mathbf{U}_k, \sqrt{t} (\check{\mathbf{A}}_t - \mathbf{A}) \right\rangle.$$

Let $\mathbf{\Lambda}$ in Equation (A.1) be $\sum_{k \in K} \langle \mathbf{\Lambda}', \mathbf{U}_k \rangle \mathbf{U}_k$, then

$$\langle \mathbf{\Lambda}', \sqrt{t} (\widehat{\mathbf{A}}_t - \mathbf{A}) \rangle \xrightarrow{d} \mathcal{N}(0, \text{vec}(\mathbf{\Lambda}')^\top \boldsymbol{\Sigma}_{\mathcal{G}} \text{vec}(\mathbf{\Lambda}')).$$

Use Cramér-Wold theorem again, we can get the theorem result. The distribution in this **Theorem** is degenerate. ■

Proof of Corollary 3.1.1. The proof is an adaption of Lütkepohl [11, Section 3.6], based on the result in **Theorem 3.1.**. We first construct the following matrix:

$$\mathbf{C} = \begin{pmatrix} \vdots \\ \text{svec}(\mathbf{u}_{i_k} \mathbf{u}_{j_k}^\top)^\top \\ \vdots \end{pmatrix} \in \mathbb{R}^{P \times \frac{N(N-1)}{2}}. \quad (\text{A.5})$$

Then test H_0 versus H_1 equals to

$$H'_0 : \mathbf{C} \text{svec}(\mathbf{A}_N) = 0 \text{ versus } H'_1 : \mathbf{C} \text{svec}(\mathbf{A}_N) \neq 0.$$

Following **Theorem 3.1.**, we have

$$\sqrt{t} \mathbf{C} \text{svec}(\widehat{\mathbf{A}}_{N,t} - \mathbf{A}_N) \xrightarrow{d} \mathcal{N}(0, \mathbf{C} \boldsymbol{\Sigma}_N \mathbf{C}^\top).$$

Hence, when H'_0 holds,

$$\sqrt{t} \mathbf{C} \text{svec}(\widehat{\mathbf{A}}_{N,t}) \xrightarrow{d} \mathcal{N}(0, \mathbf{C} \boldsymbol{\Sigma}_N \mathbf{C}^\top).$$

Then by Proposition C.2 (4) in [11], we have

$$\sqrt{t} \left[\mathbf{C} \widehat{\boldsymbol{\Sigma}}_{N,t} \mathbf{C}^\top \right]^{-\frac{1}{2}} \mathbf{C} \text{svec}(\widehat{\mathbf{A}}_{N,t}) \xrightarrow{d} \mathcal{N}(0, \mathbf{I}_P),$$

where $\widehat{\boldsymbol{\Sigma}}_{N,t} = \sum_{\substack{1 \leq l < h \leq N \\ 1 \leq l' < h' \leq N}} c_N^4 \tilde{\mathbf{u}}_{lh}^\top \widehat{\boldsymbol{\Sigma}}_{ols,t} \tilde{\mathbf{u}}_{l'h'} \text{svec}(\mathbf{u}_l \mathbf{u}_h^\top) \text{svec}(\mathbf{u}_{l'} \mathbf{u}_{h'}^\top)^\top$ is the consistent estimator of $\boldsymbol{\Sigma}_N$. Then by continuous mapping theorem:

$$t \hat{\alpha}_t^\top \left[\mathbf{C} \widehat{\boldsymbol{\Sigma}}_{N,t} \mathbf{C}^\top \right]^{-1} \hat{\alpha}_t \xrightarrow{d} \chi^2(P).$$

Note that $\mathbf{C} \text{svec}(\widehat{\mathbf{A}}_{N,t}) = \hat{\alpha}_t$, and $\{\text{svec}(\mathbf{u}_l \mathbf{u}_h^\top)\}_{l < h}$ are orthonormal basis in $\mathbb{R}^{\frac{N(N-1)}{2}}$, thus we have $\left(\mathbf{C} \widehat{\boldsymbol{\Sigma}}_{N,t} \mathbf{C}^\top \right)_{k,k'} = c_N^4 \tilde{\mathbf{u}}_{i_k j_k}^\top \widehat{\boldsymbol{\Sigma}}_{ols,t} \tilde{\mathbf{u}}_{i_{k'} j_{k'}} = \left(\widehat{\boldsymbol{\Sigma}}_{W,t} \right)_{k,k'}$. ■

B Proof of Proposition 4.1

From Definition (4.5), we have

$$\widehat{\mathbf{\Gamma}}_t(0) = \sum_{m=0}^{M-1} \frac{p_{m,t}}{t} \left(\frac{\sum_{\tau \in I_{m,t}} \mathbf{x}_{\tau-1} \mathbf{x}_{\tau-1}^\top}{p_{m,t}} - \mathbf{x}_{m-1,t} \mathbf{x}_{m-1,t}^\top \right) = \frac{\sum_{\tau=1}^t \mathbf{x}_{\tau-1} \mathbf{x}_{\tau-1}^\top}{t} - \sum_{m=0}^{M-1} \frac{p_{m,t}}{t} (\mathbf{x}_{m-1,t} \mathbf{x}_{m-1,t}^\top).$$

Plug $\mathbf{x}_t = \mathbf{b}_t^0 + \mathbf{x}'_t$ in the last equation above, we can get the formula only with respect with \mathbf{x}'_t :

$$\widehat{\mathbf{\Gamma}}_t(0) = \widehat{\mathbf{\Gamma}}_t(0)' - \sum_{m=0}^{M-1} \frac{p_{m,t}}{t} (\mathbf{x}'_{m-1,t} [\mathbf{x}'_{m-1,t}]^\top), \text{ where } \mathbf{x}'_{m-1,t} = \sum_{\tau \in I_{m,t}} \frac{\mathbf{x}'_{\tau-1}}{p_{m,t}}, \quad m = 0, \dots, M-1,$$

and $\widehat{\mathbf{\Gamma}}_t(0)' := \frac{\sum_{\tau=1}^t \mathbf{x}'_{\tau-1} [\mathbf{x}'_{\tau-1}]^\top}{t}$. Similarly, denote $\frac{\sum_{\tau=1}^t \mathbf{x}'_{\tau} [\mathbf{x}'_{\tau-1}]^\top}{t}$ by $\widehat{\mathbf{\Gamma}}_t(1)'$, we have $\widehat{\mathbf{\Gamma}}_t(1) = \widehat{\mathbf{\Gamma}}_t(1)' - \sum_{m=0}^{M-1} \frac{p_{m,t}}{t} (\bar{\mathbf{x}}'_{m,t} [\mathbf{x}'_{m-1,t}]^\top)$, with $\bar{\mathbf{x}}'_{m,t} = \sum_{\tau \in I_{m,t}} \frac{\mathbf{x}'_{\tau}}{p_{m,t}}$, $m = 0, \dots, M-1$. Since $\{\mathbf{x}'_t\}$ is the causal solution of VAR (2.1), we have

$$\begin{aligned} \text{(a')} \quad & \widehat{\mathbf{\Gamma}}_t(0)' \xrightarrow{p} \mathbf{\Gamma}(0), \quad \widehat{\mathbf{\Gamma}}_t(1)' \xrightarrow{p} \mathbf{\Gamma}(1), \\ \text{(b')} \quad & \widehat{\mathbf{\Gamma}}_t(1)' \left[\widehat{\mathbf{\Gamma}}_t(0)' \right]^{-1} \xrightarrow{p} \mathbf{\Gamma}(1) [\mathbf{\Gamma}(0)]^{-1} = \mathbf{A}, \\ \text{(c')} \quad & \sqrt{t} \text{vec} \left(\widehat{\mathbf{\Gamma}}_t(1)' \left[\widehat{\mathbf{\Gamma}}_t(0)' \right]^{-1} - \mathbf{A} \right) \xrightarrow{d} \mathcal{N}(0, [\mathbf{\Gamma}(0)]^{-1} \otimes \mathbf{\Sigma}). \end{aligned}$$

Thus, to reach the results in Proposition 4.1, we need additionally the asymptotic properties of sample mean $\bar{\mathbf{x}}'_{m,t}$, which are given in Lemma B.1.

Lemma B.1. (CLT of $\bar{\mathbf{x}}'_{m,t}$)

$$\sqrt{p_{m,t}} \bar{\mathbf{x}}'_{m,t} \xrightarrow{d} \mathcal{N}(0, \mathbf{\Phi} \mathbf{\Sigma}_M \mathbf{\Phi}^\top), \quad \forall m = 0, \dots, M-1,$$

where $\mathbf{\Phi} = (\mathbf{I}_{NF} - \mathbf{A}^M)^{-1}$, and $\mathbf{\Sigma}_M = \sum_{h=0}^{M-1} \mathbf{A}^h \mathbf{\Sigma} (\mathbf{A}^h)^\top$. Therefore, $\bar{\mathbf{x}}'_{m,t} \xrightarrow{p} 0$.

Proof of Lemma B.1. Because of the periodicity, $\{\mathbf{x}'_\tau\}_{\tau \in I_{m,\infty}}$ is also a stationary process from VAR: $\tilde{\mathbf{x}}_{t'} = \mathbf{A}^M \tilde{\mathbf{x}}_{t'-1} + \tilde{\mathbf{z}}_{t'}$, with $\tilde{\mathbf{z}}_{t'} \sim \text{IID}(0, \mathbf{\Sigma}_M)$, for all $m = 0, \dots, M-1$. Thus, apply Proposition 3.3 in Lütkepohl [11], we get the result. ■

Proof of Proposition 4.1.

$$\begin{aligned} \text{(a)} \quad & \text{When } t \rightarrow \infty, \widehat{\mathbf{\Gamma}}_t(0) = \widehat{\mathbf{\Gamma}}_t(0)' - \sum_{m=0}^{M-1} \frac{1}{M} (\bar{\mathbf{x}}'_{m,t} [\bar{\mathbf{x}}'_{m,t}]^\top) \xrightarrow{p} \mathbf{\Gamma}(0) - 0 = \mathbf{\Gamma}(0), \text{ and } \widehat{\mathbf{\Gamma}}_t(1) = \\ & \widehat{\mathbf{\Gamma}}_t(1)' - \sum_{m=0}^{M-1} \frac{1}{M} (\bar{\mathbf{x}}'_{m,t} [\bar{\mathbf{x}}'_{m-1,t}]^\top) \xrightarrow{p} \mathbf{\Gamma}(1), \text{ with } \bar{\mathbf{x}}'_{-1,t} := \bar{\mathbf{x}}'_{M-1,t}. \end{aligned}$$

(b) From trend model (4.3), $\bar{\mathbf{x}}_{m,t} = \frac{\sum_{\tau \in I_{m,t}} \mathbf{b}_m^0 + \mathbf{x}'_{\tau}}{p_{m,t}} = \mathbf{b}_m^0 + \bar{\mathbf{x}}'_{m,t} \xrightarrow{p} \mathbf{b}_m^0, \forall m = 0, \dots, M-1$. Since asymptotically, $\bar{\mathbf{x}}_{m,t} = \underline{\mathbf{x}}_{m,t}$, thus both means can be used to estimate \mathbf{b}_m^0 . On the other hand, based on (a), using continuous mapping theorem on the matrix inverse, we have $\check{\mathbf{A}}_t = \hat{\mathbf{\Gamma}}_t(1) \left[\hat{\mathbf{\Gamma}}_t(0) \right]^{-1} \xrightarrow{p} \mathbf{A}$.

(c) When $t \rightarrow \infty$, $\check{\mathbf{A}}_t = \left[\hat{\mathbf{\Gamma}}_t(1)' - \sum_{m=0}^{M-1} \frac{p_{m,t}}{t} \left(\bar{\mathbf{x}}'_{m,t} [\bar{\mathbf{x}}'_{m-1,t}]^{\top} \right) \right] \left[\hat{\mathbf{\Gamma}}_t(0)' - \sum_{m=0}^{M-1} \frac{p_{m,t}}{t} \left(\bar{\mathbf{x}}'_{m-1,t} [\bar{\mathbf{x}}'_{m-1,t}]^{\top} \right) \right]^{-1}$.

Use the Woodbury formula on the matrix inverse, we have

$$\begin{aligned} \sqrt{t}(\check{\mathbf{A}}_t - \mathbf{A}) &= \sqrt{t}(\hat{\mathbf{\Gamma}}_t(1)' \left[\hat{\mathbf{\Gamma}}_t(0)' \right]^{-1} - \mathbf{A}) - \sqrt{t} \sum_{m=0}^{M-1} \frac{p_{m,t}}{t} \left(\bar{\mathbf{x}}'_{m,t} [\bar{\mathbf{x}}'_{m-1,t}]^{\top} \right) \left[\hat{\mathbf{\Gamma}}_t(0)' \right]^{-1} \\ &\quad + \frac{\sqrt{t}}{1-g} \hat{\mathbf{\Gamma}}_t(1)' \left[\hat{\mathbf{\Gamma}}_t(0)' \right]^{-1} \sum_{m=0}^{M-1} \frac{p_{m,t}}{t} \left(\bar{\mathbf{x}}'_{m-1,t} [\bar{\mathbf{x}}'_{m-1,t}]^{\top} \right) \left[\hat{\mathbf{\Gamma}}_t(0)' \right]^{-1} \\ &\quad - \frac{\sqrt{t}}{1-g} \sum_{m=0}^{M-1} \frac{p_{m,t}}{t} \left(\bar{\mathbf{x}}'_{m,t} [\bar{\mathbf{x}}'_{m-1,t}]^{\top} \right) \left[\hat{\mathbf{\Gamma}}_t(0)' \right]^{-1} \sum_{m=0}^{M-1} \frac{p_{m,t}}{t} \left(\bar{\mathbf{x}}'_{m-1,t} [\bar{\mathbf{x}}'_{m-1,t}]^{\top} \right) \left[\hat{\mathbf{\Gamma}}_t(0)' \right]^{-1}, \end{aligned}$$

where, $g = \text{tr} \left(\sum_{m=0}^{M-1} \frac{p_{m,t}}{t} \left(\bar{\mathbf{x}}'_{m-1,t} [\bar{\mathbf{x}}'_{m-1,t}]^{\top} \right) \left[\hat{\mathbf{\Gamma}}_t(0)' \right]^{-1} \right)$. Based on the result of (c'), to reach the same asymptotic distribution, we only need to show that, the reminder terms, namely from the second term to the last term above, all converge to 0 in probability.

From Slutsky's theorem and Lemma B.1, we have the asymptotic result:

$$\forall m, \frac{p_{m,t}}{\sqrt{t}} \left(\bar{\mathbf{x}}'_{m,t} [\bar{\mathbf{x}}'_{m-1,t}]^{\top} \right) = \frac{1}{\sqrt{M}} \left(\sqrt{p_{m,t}} \bar{\mathbf{x}}'_{m,t} \right) [\bar{\mathbf{x}}'_{m-1,t}]^{\top} \xrightarrow{p} 0.$$

Thus, $\sqrt{t} \sum_{m=0}^{M-1} \frac{p_{m,t}}{t} \left(\bar{\mathbf{x}}'_{m,t} [\bar{\mathbf{x}}'_{m-1,t}]^{\top} \right) \left[\hat{\mathbf{\Gamma}}_t(0)' \right]^{-1} \xrightarrow{p} 0$. Similarly, $\sqrt{t} \sum_{m=0}^{M-1} \frac{p_{m,t}}{t} \left(\bar{\mathbf{x}}'_{m-1,t} [\bar{\mathbf{x}}'_{m-1,t}]^{\top} \right) \left[\hat{\mathbf{\Gamma}}_t(0)' \right]^{-1} \xrightarrow{p} 0$.

Since, it is obvious that $\sum_{m=0}^{M-1} \frac{p_{m,t}}{t} \left(\bar{\mathbf{x}}'_{m-1,t} [\bar{\mathbf{x}}'_{m-1,t}]^{\top} \right) \xrightarrow{p} 0$, then use the properties of convergence in probability and continuous mapping theorem, we can show the reminder terms all converge to 0 in probability. ■

C Optimality conditions of $L_{\lambda_{t+1},t}(\dots, 1, \mu_i, 0, \dots)$ for $\mathbf{A}_{\lambda_{t+1},t}(\dots, 1, \mu_i, 0, \dots)$

$$\begin{cases} \mathbf{\Gamma}_0^1(\mu_i) \mathbf{a}_1^s - \gamma_1^1(\mu_i) + \left(1 + \frac{1}{t}\right) \sqrt{2F} \lambda_{t+1} \mathbf{w}_1 = 0 \\ \mathbf{\Gamma}_0^0(\mu_i) \mathbf{a}_1^s - \gamma_1^0(\mu_i) + \left(1 + \frac{1}{t}\right) \sqrt{2F} \lambda_{t+1} \mathbf{w}_0 = 0, \end{cases} \quad (\text{C.1})$$

where we define $\mathbf{a}_1^s, K_N^1, K_N^0, K^1, \mathbf{w}_1, \mathbf{w}_0$ the same way as Proposition 3.2, yet related to $\mathbf{A}_{\lambda_{t+1}, t}(\mu_1, \dots, \mu_{NF})$,

$$\begin{aligned}\Gamma_0(\mu_i) &= \Gamma_0 + \frac{1}{t} \sum_{n=1}^{i-1} \frac{p_{\bar{m}, t}}{p_{\bar{m}, t} + 1} [\tilde{\mathbf{X}}_t - \tilde{\mathbf{X}}_{\bar{m}-1, t}]_{:, n} [\tilde{\mathbf{X}}_t - \tilde{\mathbf{X}}_{\bar{m}-1, t}]_{:, n}^\top + \frac{\mu_i}{t} \frac{p_{\bar{m}, t}}{p_{\bar{m}, t} + \mu_i} [\tilde{\mathbf{X}}_t - \tilde{\mathbf{X}}_{\bar{m}-1, t}]_{:, i} [\tilde{\mathbf{X}}_t - \tilde{\mathbf{X}}_{\bar{m}-1, t}]_{:, i}^\top, \\ \gamma_1(\mu_i) &= \gamma_1 + \frac{1}{t} \sum_{n=1}^{i-1} \frac{p_{\bar{m}, t}}{p_{\bar{m}, t} + 1} (\mathbf{x}_{t+1, n} - (\mathbf{x}_{\bar{m}, t})_n) [\tilde{\mathbf{X}}_t - \tilde{\mathbf{X}}_{\bar{m}-1, t}]_{:, n} + \frac{\mu_i}{t} \frac{p_{\bar{m}, t}}{p_{\bar{m}, t} + \mu_i} (\mathbf{x}_{t+1, i} - (\mathbf{x}_{\bar{m}, t})_i) [\tilde{\mathbf{X}}_t - \tilde{\mathbf{X}}_{\bar{m}-1, t}]_{:, i},\end{aligned}$$

with $(\tilde{\mathbf{X}}_{\bar{m}-1, t})_{k, i} = c_k[\mathbf{U}_k]_{i, : \bar{m}-1, t}$, $p_{\bar{m}, t} := t \bmod M$, Γ_0, γ_1 the same as Proposition 4.2,
 $\gamma_1^1(\mu_i) = [\gamma_1(\mu_i)]_{K^1}$, $\gamma_1^0(\mu_i) = [\gamma_1(\mu_i)]_{K_N^0}$, $\Gamma_0^1(\mu_i) = [\Gamma_0(\mu_i)]_{K^1}$, $\Gamma_0^0(\mu_i) = [\Gamma_0(\mu_i)]_{K_N^0, K^1}$.